

Balancing Error and Dissipation in Highly-Reliable Computing

Paul M. Riechers* and Alexander B. Boyd†

*Complexity Institute and School of Physical and Mathematical Sciences,
Nanyang Technological University, 637371 Singapore, Singapore*

Gregory W. Wimsatt‡ and James P. Crutchfield§

*Complexity Sciences Center and Physics Department,
University of California at Davis, One Shields Avenue, Davis, CA 95616*

(Dated: March 3, 2022)

Modern digital electronics support remarkably reliable computing, especially given the challenge of controlling nanoscale logical components that interact in fluctuating environments. However, the high-reliability limit is subject to a fundamental error–energy–efficiency tradeoff that arises from time-symmetric control. Requiring a low probability of error causes energy consumption to diverge as logarithm of the inverse error rate for nonreciprocal logical transitions. The *reciprocity* (*self-invertibility*) of a computation is a stricter condition for thermodynamic efficiency than logical reversibility (*invertibility*), the latter being the root of Landauer’s work bound. In fact, the average energy required for reliable erasure is well above that bound. Explicit simulations of work production closely track the error-dissipation tradeoff, diverging from the Landauer bound as the error rate decreases. And, unlike the Landauer work, which can be recovered, the nonreciprocal work must be irreversibly dissipated. Analogous bounds hold for the universal NAND gate and extend to circuits of logical gates. That said, strictly-reciprocal logic gates, such as communication relays and NOT gates, are exempt and can be efficiently implemented via time-symmetric protocols. For all other computations, though, time-asymmetric control must be used to avoid dissipation arising from nonreciprocity. The lesson is that highly-reliable computation under time-symmetric control cannot reach, and is often far above, the Landauer limit. In this way, time-asymmetry becomes a design principle for thermodynamically-efficient computing. We also demonstrate that the time-reversal symmetries of the memory elements themselves play an essential role in determining the minimal energy necessary to implement a computation. Beyond engineered computation, the results reveal a generic error–dissipation tradeoff in steady-state transformations of genetic information as carried out by biological organisms.

Keywords: nonequilibrium steady state, thermodynamics, dissipation, entropy production, Landauer bound

CONTENTS

I. Introduction	2	1. Two-state rate equations	15
II. Computational Dissipation	3	2. Underdamped double-well potential	16
A. Partial Knowledge	4	B. Logic Gates	18
B. Thermodynamic Computing	5	C. Dissipation in Biological Processing	18
C. Metastable Processing	7	V. Conclusion	20
D. Time Symmetric Driving	8	A. Related Results	20
E. (Non)Reciprocity	9	B. Looking Forward	21
F. Time Symmetric Memory	10	Acknowledgments	21
III. Almost-Deterministic Computing	11	A. Dissipated-work bounds	22
IV. Applications	13	1. General observation channels	22
A. Erasure	13	2. Computational coarse-grainings	24
		B. Dissipated-work bound for computation	24
		C. Transition-specific fluctuation theorem	27
		D. Four cases	28
		E. Langevin dynamics for erasure	29

* pmriechers@gmail.com

† abboyd@ucdavis.edu

‡ gwwimsatt@ucdavis.edu

§ chaos@ucdavis.edu

F. Minimal dissipation in the time-symmetric universal NAND gate	30
References	32

I. INTRODUCTION

Tantalizingly, the thermodynamics of computation tells us that information processing can be achieved with zero energy dissipation ... if one has sufficient control over a system's microscopic degrees of freedom and can endure the quasistatic limit of infinitely-slow processing [1–5]. To be useful, though, computation must be performed in finite time. Unfortunately, this requires additional work and guarantees the investment is lost via dissipation. This state of affairs poses a grand challenge to thermodynamic computing: Identify control protocols that reliably drive a system between memory states according to a desired computation in finite time and with minimal dissipation. Failing an answer, the fundamental physical limits on computation remain elusive.

In point of fact, contemporary finite-time thermodynamics predicts that energy-efficient protocols of duration τ entail dissipation that scales as τ^{-1} [6–11]. That is, reliable computation could be performed with arbitrarily little dissipation at the cost of arbitrarily slow processing.

An obvious and common implementation of finite-time computation is to ramp up a set of forces¹ that transform previously-metastable memories according to the computation's map. At an appropriate later time, the forces are ramped down (mirroring the ramp-up procedure) so that the computing system returns to its resting state, while new memories are again stored robustly in metastable configurations. Such implementations represent control protocols that are symmetric in time.

More to the point, time-symmetric protocols are common. Most notably, the primary signal controlling information processing in contemporary microprocessors is a time-symmetric clock-voltage signal—a several gigahertz square wave that orchestrates all transformations of the computer's logic and memory components [12, 13].

Time-symmetric protocols are also common in other settings that seek reliable transformations. In recent experiments on synthetic molecular machines, molecular rotors are externally driven by a time-symmetric (sinusoidal)

electric field. And, new autonomous synthetic molecular machines reliably produce steady-state rotations despite a time-*invariant* (a special case of time-symmetric) nonequilibrium environment [14]. They achieve this through chemical catalysis, much as natural molecular machines operate in vivo. In vivo, reliable genetic transformation of DNA (and reliable directional motion of molecular motors) occurs in an environment with very low Reynolds number, where there are no inertial variables to freely exert a time-asymmetric influence [15, 16]. More broadly, breaking time symmetry in Brownian motion *requires* significant dissipation [17]. And so, in both the biological and engineered worlds, simple time-symmetric protocol design—turning on and then turning off an interaction—seems to offer an energetically-efficient and reliable way to implement change.

The goal, naturally enough, is to implement information processing in ways that require no more than the minimal work exertion set by Landauer's logical-irreversibility bound [18]: $W \geq k_B T \ln 2$. One might even hope that this work could then be recycled rather than dissipated. Indeed, as appreciated recently, changes in the nonequilibrium addition to free energy can be leveraged to implement logically-irreversible computations in a thermodynamically reversible manner [2–5]. The vision is of a future of hyper-efficient computing using orders-of-magnitude less energy than currently.

However, there is a wrinkle in this optimism. *All* time-symmetric protocols for transforming metastable memories engender an irreducible trade-off between computational accuracy and energy efficiency. Specifically, in the limit of highly-reliable computing with vanishingly-small error probability ϵ , the minimal dissipation under time-symmetric controls diverges as $-\ln \epsilon$ with a coefficient proportional to the computation's *nonreciprocity*—the nonself-invertibility of its memory-state transitions.

For reliable time-symmetric implementations of a deterministic computation \mathcal{C} , which maps each memory state $m \mapsto \mathcal{C}(m)$, the minimal work above the change in local-equilibrium free energy is $k_B T \ln(1/\epsilon)$ whenever $\mathcal{C}(\mathcal{C}(m)) \neq m$. That is, work $k_B T \ln(1/\epsilon)$ is required whenever the computation iterated twice does not return to the original memory state. Moreover, there is a correction when time-odd variables store memory that highlights the unique advantages of both magnetic and conformational memories.

In this way, nonreciprocity identifies a dominant cost of thermodynamic computing for the broad class of time-symmetric control protocols. Future work will address more general thermodynamic implications of reliable computation. However, since time-symmetric control protocols are common and often unavoidable in key applica-

¹ For example, a set of gate voltages may be applied or, by any other method, a potential energy landscape may be altered to temporarily couple and bias a set of initially-independent metastable potential minima.

tions, they are the subject of our error–dissipation tradeoff analysis here.

The first step in our development revisits the basics of dissipation in thermodynamic systems and the effect of partial knowledge, when the entire microstate cannot be observed or controlled. These dissipation costs are then recast to broadly apply to thermodynamic computing and, in particular, information storage and processing in metastable mesoscopic states. We then analyze the role of time symmetries in control protocols and give a thermodynamic accounting. Dissipation scaling with error level is derived and applied in the limit of highly-reliable computing. This is then used to analyze dissipation in erasure, logic gates, and biological systems. We conclude, briefly comparing recent work on control restrictions, and noting directions for further exploration. Appendices provide details underlying the theory and simulations.

II. COMPUTATIONAL DISSIPATION

To start, consider any physical realization of a memory device with a system Hamiltonian \mathcal{H}_x parametrized by control $x \in \mathcal{X}$. For example, x could correspond to an applied electromagnetic field, a vector of quantities specifying a potential energy landscape, or a set of piston positions. The Hamiltonian \mathcal{H}_x determines the system’s instantaneous energies $\{E_x(s)\}_{s \in \mathcal{S}}$, where \mathcal{S} is the set of system microstates. We assume that the system is in contact with an effectively memoryless heat bath at temperature T that enables the system to relax to both local and global equilibria. The instantaneous stochastic microstate dynamics are completely determined by the system’s instantaneous Hamiltonian and the system’s interaction with the heat bath. Work is performed by driving the system via a *control protocol* $x_{0:\tau} = x_0 \cdots x_\tau$, which is the trajectory of the control parameters from time 0 to τ . The work W measures the accumulated change in the energy of occupied microstates—energy that was supplied by the controller. In the following, we are especially interested in *computations* implemented by the control protocol and in the associated work cost.

Understanding the relationship between work costs and computations requires tracking the energetics of microstate trajectories $s_{0:\tau} = s_0 \cdots s_\tau$ of the system from time 0 to τ . Via the implied dynamics set by the time-dependent Hamiltonian \mathcal{H}_{x_t} and the coupling with the bath at temperature T , the initial state s_0 and the control protocol $x_{0:\tau}$ determine the probability of microstate

trajectories:

$$\begin{aligned} \Pr_{x_{0:\tau}}(\mathcal{S}_{0:\tau} = s_{0:\tau} | \mathcal{S}_0 = s_0) \\ \equiv \Pr(\mathcal{S}_{0:\tau} = s_{0:\tau} | \mathcal{S}_0 = s_0, \mathcal{X}_{0:\tau} = x_{0:\tau}) , \end{aligned} \quad (1)$$

where \mathcal{S}_t is the random variable for the microstate at time t and $\mathcal{S}_{0:\tau}$ is the random variable chain for the full state trajectory. The subscripted probability $\Pr_{x_{0:\tau}}(\cdot)$ denotes the probability distribution *induced* by the driving protocol $x_{0:\tau}$. This is the same as the probability *conditioned* on the driving protocol, as described by Eq. (1).

Hamiltonian control implies microscopic reversibility of the instantaneous microstate dynamics. This means state trajectories that release energy into the heat bath ($Q > 0$) are exponentially more likely than the time-reversed microstate trajectory (that absorb heat), if the protocol were run in reverse [19–21]. Specifically:

$$\frac{\Pr_{x_{0:\tau}}(\mathcal{S}_{0:\tau} = s_{0:\tau} | \mathcal{S}_0 = s_0)}{\Pr_{\mathbf{J}(x_{0:\tau})}(\mathcal{S}_{0:\tau} = \mathbf{J}(s_{0:\tau}) | \mathcal{S}_0 = s_\tau^\dagger)} = e^{\beta Q(s_{0:\tau}, x_{0:\tau})} ,$$

where $\beta = (k_B T)^{-1}$ and k_B is Boltzmann’s constant. \mathbf{J} denotes time-reversal, including not only reversal of the time ordering, but also conjugation of time-odd variables such as momentum and spin: $s_0 \cdots s_\tau \mapsto s_\tau^\dagger \cdots s_0^\dagger$. For example, if the microstate $s = (\vec{q}, \vec{\varphi})$ is a collection of spatial \vec{q} and momentum $\vec{\varphi}$ degrees of freedom, then the conjugation simply flips all of the momentum degrees of freedom $s^\dagger = (\vec{q}, -\vec{\varphi})$.

Thermodynamic irreversibility is quantified by *entropy production* Σ . The second law of thermodynamics says that entropy production is expected to be nonnegative: $\langle \Sigma \rangle \geq 0$. In our setting, Σ is simply the net change in the component entropies of both the system and the bath. More specifically, entropy production decomposes into the change in heat-bath entropy $Q(s_{0:\tau}, x_{0:\tau})/T$ beyond any compensating reduction in the system’s microstate entropy. The system’s instantaneous microstate entropy is given by the nonequilibrium *surprisal* $-k_B \ln \boldsymbol{\mu}_t(s_t)$, where $\boldsymbol{\mu}_t(s_t) = \Pr_{x_{-\infty:t}}(\mathcal{S}_t = s_t)$ is the current microstate’s probability given the *entire history* of preparation and driving [20, 22, 23].² Accordingly, the entropy production is:

$$\Sigma = \frac{1}{T} Q(s_{0:\tau}, x_{0:\tau}) + \Delta(-k_B \ln \boldsymbol{\mu}_t(s_t)) ,$$

² Hence, $\boldsymbol{\mu}_t(s_t)$ is the expected probability of being in the actual microstate s_t over many trials where the system is prepared and driven in exactly the same way. The fact that this distribution is not δ -distributed is due to the stochasticity induced by the interaction with the heat bath (and any other uncontrollable degrees of freedom).

where Δ indicates the change from time 0 to τ . Specifically, μ_0 is the distribution over microstates given the system's initial preparation and μ_τ is the time-evolved version of μ_0 under the influence of the driving $x_{0:\tau}$. This results in the trial-specific entropy production [19–21]:

$$\begin{aligned}\Sigma &= \frac{1}{T} Q(s_{0:\tau}, x_{0:\tau}) + k_B \ln \frac{\mu_0(s_0)}{\mu_\tau(s_\tau)} \\ &= k_B \ln \left(\frac{\Pr_{x_{0:\tau}}(\mathcal{S}_{0:\tau} = s_{0:\tau} | \mathcal{S}_0 = s_0) \mu_0(s_0)}{\Pr_{\mathbf{H}(x_{0:\tau})}(\mathcal{S}_{0:\tau} = \mathbf{H}(s_{0:\tau}) | \mathcal{S}_0 = s_0^\dagger) \mu_\tau(s_\tau)} \right) \\ &= k_B \ln \left(\frac{\Pr_{x_{0:\tau}}(\mathcal{S}_{0:\tau} = s_{0:\tau} | \mathcal{S}_0 \sim \mu_0)}{\Pr_{\mathbf{H}(x_{0:\tau})}(\mathcal{S}_{0:\tau} = \mathbf{H}(s_{0:\tau}) | \mathcal{S}_0 \sim \mu_\tau^\dagger)} \right), \quad (2)\end{aligned}$$

where μ_τ^\dagger is the distribution such that $\mu_\tau^\dagger(s) = \mu_\tau(s^\dagger)$. The condition $\mathcal{S}_0 \sim \mu$ means the random variable \mathcal{S}_0 is distributed according to μ , as in Ref. [24]. We used the fact that $\mu_\tau(s) = \mu_\tau^\dagger(s^\dagger)$ in going from the second to the third line.

When all influences driving the system away from equilibrium are controlled changes to the system Hamiltonian, the total entropy production is proportional to the *dissipated work* W_{diss} , which is the accumulation of lost opportunities to extract work:

$$W_{\text{diss}} = T\Sigma.$$

The entropy production and dissipated work both measure a given computation's efficiency, as they both quantify the degree to which more work was done than necessary by an unrestricted controller.

The *expected* dissipated work quantifies the difference between the average amount of work done beyond the change in nonequilibrium free energy [25]:

$$\langle W_{\text{diss}} \rangle = \langle W \rangle - \Delta \mathcal{F}. \quad (3)$$

This is the average work that has been irreversibly lost, since the nonequilibrium free energy \mathcal{F} is the expected amount of energy that possibly could be extracted as work [26]. Calculating the dissipated work from these two quantities seems to require explicit knowledge of the Hamiltonian, since the work is the integrated change in the energy due to changes in control:

$$\langle W \rangle = \sum_s \int_0^\tau dt \mu_t(s) \frac{\partial E_{x_t}(s)}{\partial x_t} \frac{dx_t}{dt},$$

and the nonequilibrium free energy is the difference between the average energy and the microstate entropy [26]:

$$\mathcal{F}(t) = \langle \mathcal{H}_{x_t} \rangle - k_B T H(\mathcal{S}_t),$$

where $H(Z) = -\sum_z \Pr(Z = z) \ln \Pr(Z = z)$ is the Shan-

non entropy of the driven system in nats.³

However, due to Eq. (2), we can calculate the dissipated work for a control protocol using only the probability of forward trajectories under forward driving $\rho(\mathcal{S}_{0:\tau} = s_{0:\tau}) = \Pr_{x_{0:\tau}}(\mathcal{S}_{0:\tau} = s_{0:\tau} | \mathcal{S}_0 \sim \mu_0)$ and reverse microstate trajectories under reverse driving $\rho^R(\mathcal{S}_{0:\tau} = s_{0:\tau}) = \Pr_{\mathbf{H}(x_{0:\tau})}(\mathcal{S}_{0:\tau} = \mathbf{H}(s_{0:\tau}) | \mathcal{S}_0 \sim \mu_\tau^\dagger)$. Averaging over forward trajectories produces a relative entropy:

$$\begin{aligned}\beta \langle W_{\text{diss}} \rangle &= \sum_{s_{0:\tau}} \rho(\mathcal{S}_{0:\tau} = s_{0:\tau}) \ln \frac{\rho(\mathcal{S}_{0:\tau} = s_{0:\tau})}{\rho^R(\mathcal{S}_{0:\tau} = s_{0:\tau})} \\ &= D_{\text{KL}} [\rho(\mathcal{S}_{0:\tau}) \parallel \rho^R(\mathcal{S}_{0:\tau})], \quad (4)\end{aligned}$$

where $D_{\text{KL}}[\cdot \parallel \cdot]$ is the Kullback–Leibler divergence [27–29].

A. Partial Knowledge

This powerful relation leads to bounds on dissipated work based on *observed trajectories*, which contain only partial details of the full microstate trajectory. And, expressing the dissipated work and entropy production in terms of the relative entropy between forward and reverse trajectories, it provides a method to reconstruct a system's thermodynamics without explicit knowledge of the underlying Hamiltonian mechanics. This only requires knowledge of trajectory probabilities under forward and reverse driving and these can be determined experimentally.

However, practical considerations can stand in the way. Often direct observations of a thermodynamic system's underlying microstate trajectories are not available. Then, instead, one acquires data on some observable \vec{y} .⁴ The following treats \vec{y} as the system's observed trajectory. This can be much simpler than the system's microstate

³ In point of fact, knowledge of the Hamiltonian is not strictly necessary if one instead calculates $\langle W_{\text{diss}} \rangle = \langle W_{\text{ex}} \rangle - \Delta \mathcal{F}_{\text{add}}$, where $W_{\text{ex}} = W - \Delta F_x^{\text{eq}}$ and $\mathcal{F}_{\text{add}} = k_B T D_{\text{KL}}[\mu_t \parallel \pi_{x_t}]$. With knowledge (or observation) of the equilibrium distribution π_x associated with each control setting x , one can leverage the Boltzmann relationship $\pi_x(s) = e^{-\beta[E_x(s) - F_x^{\text{eq}}]}$ to calculate: $\beta \langle W_{\text{ex}} \rangle = \sum_s \int_0^\tau dt \mu_t(s) \frac{\partial}{\partial x_t} (-\ln \pi_{x_t}(s)) \frac{dx_t}{dt}$. Still, Eq. (4) presents an even more tempting opportunity for calculating $\langle W_{\text{diss}} \rangle$ directly from observed trajectory probabilities.

⁴ In general, observable \vec{y} could be any stochastic functional of the joint microstate trajectory $(x_{0:\tau}, s_{0:\tau})$; for example, observations of the trajectory through a noisy, lossy channel or observed values of mechanical work. In the case we observe mechanical work values $W = w$, and noting that $\mathbf{H}(w) = -w$, Eq. (6) yields a lower bound on the dissipation given far-from equilibrium work distributions: $\beta \langle W_{\text{diss}} \rangle \geq D_{\text{KL}}[\Pr_{x_{0:\tau}}(W | \mathcal{S}_0 \sim \mu_0) \parallel \Pr_{\mathbf{H}(x_{0:\tau})}(-W | \mathcal{S}_0 \sim \mu_\tau^\dagger)]$. In itself this is a quite interesting result.

trajectory $s_{0:\tau}$, which often is a high-dimensional object whose probability can be nearly impossible to estimate. Moreover, observed trajectories typically occupy a smaller space, facilitating better probability estimates. The following discusses how observed-trajectory probabilities can be used to bound dissipated work, thus circumventing the difficulty of acquiring detailed knowledge of microstate trajectories and their probabilities. This will allow us to infer new lower bounds on computational dissipation from only partial knowledge related to the logical dynamics of the computation itself.

Consider an observed trajectory measured via an *observation channel* Γ on microstate trajectories:

$$\Gamma_{s_{0:\tau}, x_{0:\tau} \rightarrow \vec{y}} = \Pr(\vec{Y} = \vec{y} | \mathcal{S}_{0:\tau} = s_{0:\tau}, \mathcal{X}_{0:\tau} = x_{0:\tau}) .$$

Then, as App. A shows, the observation-informed estimate of the dissipated work bounds the actual dissipated work. A simple and important example of an observation channel is a coarse-graining of microstate trajectories. We will use this shortly to derive our main results [27, 30, 31].

Appendix A shows that an observation channel gives the probability of observed trajectories under forward driving:

$$\begin{aligned} \rho(\vec{Y} = \vec{y}) &= \sum_{s_{0:\tau}} \Gamma_{s_{0:\tau}, x_{0:\tau} \rightarrow \vec{y}} \rho(\mathcal{S}_{0:\tau} = s_{0:\tau}) \\ &= \Pr_{x_{0:\tau}}(\vec{Y} = \vec{y} | \mathcal{S}_0 \sim \mu_0) , \end{aligned}$$

and the probability of reverse observations under reverse driving:

$$\begin{aligned} \rho^R(\vec{Y} = \vec{y}) &= \sum_{s_{0:\tau}} \Gamma_{\mathbf{J}(s_{0:\tau}), \mathbf{J}(x_{0:\tau}) \rightarrow \mathbf{J}(\vec{y})} \rho^R(\mathcal{S}_{0:\tau} = s_{0:\tau}) \\ &= \Pr_{\mathbf{J}(x_{0:\tau})}(\vec{Y} = \mathbf{J}(\vec{y}) | \mathcal{S}_0 \sim \mu_\tau^\dagger) . \end{aligned}$$

The relative entropy chain rule [24] then implies that the dissipated work is bounded below by the difference of terms:

$$\beta \langle W_{\text{diss}} \rangle \geq D_{\text{KL}} \left[\rho(\vec{Y}) \parallel \rho^R(\vec{Y}) \right] - \frac{1}{k_B} \Sigma_{\text{ch}} , \quad (5)$$

where $k_B D_{\text{KL}} \left[\rho(\vec{Y}) \parallel \rho^R(\vec{Y}) \right]$ is an estimate of entropy production that only requires the probability of observed trajectories and:

$$\begin{aligned} \Sigma_{\text{ch}} &\equiv k_B \\ &\times \left\langle D_{\text{KL}} \left[\Gamma_{s_{0:\tau}, x_{0:\tau} \rightarrow \vec{Y}} \parallel \Gamma_{\mathbf{J}(s_{0:\tau}), \mathbf{J}(x_{0:\tau}) \rightarrow \mathbf{J}(\vec{Y})} \right] \right\rangle_{\rho(\mathcal{S}_{0:\tau})} \end{aligned}$$

is the effective *channel irreversibility*. Σ_{ch} measures how much dissipation in microscopic dynamics is overestimated due to (i) dissipation in the observational channel Γ and

(ii) the definition one uses for $\mathbf{J}(\vec{y})$, if it does not correspond to physical time reversal of the observable.

Equation (5) is a general new bound on dissipation for any physical process via any observation channel. In particular, it allows us to rigorously analyze the dissipation required to implement any coarse features of a computation. While this general bound on entropy production differs from those developed for coarse-grainings in Refs. [27, 30, 31], we recover similar results in the case that the channel is reversible:

$$\Sigma_{\text{ch}} = 0 .$$

This is equivalent to $\Gamma_{s_{0:\tau}, x_{0:\tau} \rightarrow \vec{y}} = \Gamma_{\mathbf{J}(s_{0:\tau}), \mathbf{J}(x_{0:\tau}) \rightarrow \mathbf{J}(\vec{y})}$. For reversible observation channels the estimate of entropy production, obtained from forward and reverse observation sequences, bounds the dissipated work:

$$\beta \langle W_{\text{diss}} \rangle \geq D_{\text{KL}} \left[\rho(\vec{Y}) \parallel \rho^R(\vec{Y}) \right] . \quad (6)$$

For our purpose of bounding computational dissipation via the desired logical dynamics, it is sufficient to focus on the reversible channel case of Eq. (6). As we will show, this is particularly useful for metastable information processing.

Equation (6) is close to calculating an estimate for entropy production divorced from knowledge of microstate dynamics. $\Pr_{x_{0:\tau}}(\vec{Y} | \mathcal{S}_0 \sim \mu_0)$, for instance, can be recovered from tracking observation frequencies given a system's initialization μ_0 and the driving $x_{0:\tau}$. However, since $\Pr_{\mathbf{J}(x_{0:\tau})}(\vec{Y} = \mathbf{J}(\vec{y}) | \mathcal{S}_0 \sim \mu_\tau^\dagger)$ depends on initially being in distribution μ_τ^\dagger , it is unclear how to experimentally access these probabilities in the presence of time-odd variables, like momentum. Fortunately, as we now show, this obstacle can be removed for physical computations using metastable memories. Ignoring the underlying microstate dynamics and, instead, only tracking the logical dynamics, we bound the work production while computing.

B. Thermodynamic Computing

To be usefully manipulated, memories must be physically addressable. Accordingly, we define the set \mathcal{M} of *memory states* as a partition of the set \mathcal{S} of microstates, such that each memory state $m \in \mathcal{M}$ is a subset of the microstates: $m \subset \mathcal{S}$ and $\bigcup m = \mathcal{S}$. In this way, the memory state random variable \mathcal{M}_t at time t is determined by the microstate \mathcal{S}_t . Moreover, for memory states to robustly hold memories between computations, we assume that partitioning is such that each memory state corresponds to a state-space region that is effectively autonomous when no computation is being performed, resulting in metastabil-

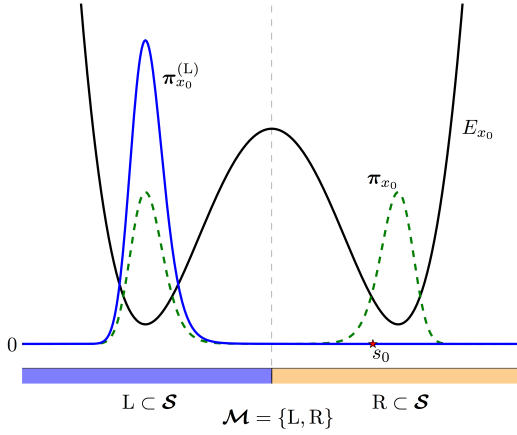


FIG. 1. Bistable memory element: A cross-section (at constant momentum φ_0) of both global and local equilibrium. Initial system state $s_0 = (q_0, \varphi_0)$ (red star) lies in a continuum. The energy landscape (black curve) has two symmetric minima that effectively partition the space into robust Left (blue) and Right (yellow) spatial memory states. The stable equilibrium distribution (green dashed curve) is uniformly distributed over the Left and Right states. The restriction of the equilibrium distribution to the Left well (blue curve) is metastable, only locally in equilibrium.

ity of the memory.⁵ Figure 1 shows a spatial system that has been partitioned into Left (L) and Right (R) memory states, each of which corresponds to a minimum in the energy landscape.

Partitioning microstates into metastable memory states \mathcal{M} introduces an observational channel Γ for monitoring computation. The task of a computation is to map an initial memory state m to a final memory state m' according to a given conditional probability distribution:

$$p(m \rightarrow m') = \Pr(\mathcal{M}_\tau = m' | \mathcal{M}_0 = m) .$$

For instance, as shown in Fig. 2 for the system of Fig. 1, erasure is composed of two desired transitions with high probabilities— $p(L \rightarrow L) \approx 1$ and $p(R \rightarrow L) \approx 1$ —between the two metastable memory states. (The latter are labeled L and R according to the common use of left and right minima in a double-well potential landscape to store a bit [32].) A computation occurs due to a particular stochastic trajectory, such as the red path shown in Fig. 2. Naturally, the statistics of the memory state transition probability $p(L \rightarrow L)$, say, come from the ensemble of trajectories. While stochasticity is the rule in physical computations, the following focuses on nearly-deterministic computations, such as highly-reliable erasure.

⁵ During a computation, though, driving couples memory states to instantiate nontrivial computing.

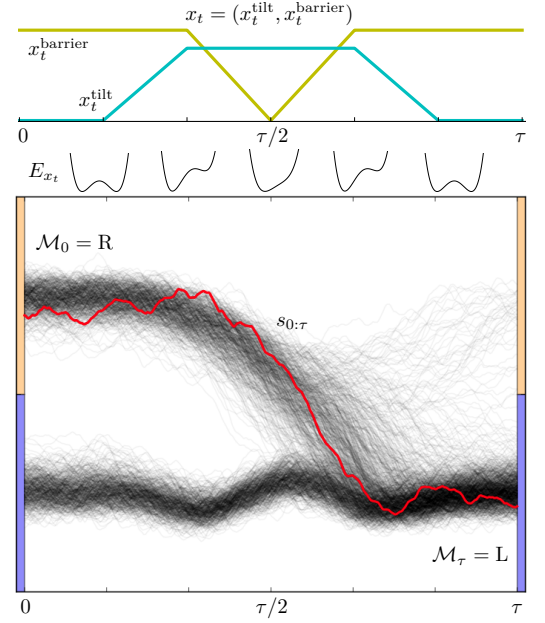


FIG. 2. (Top) Time-symmetric control implementing reliable information processing: erasure to L. (Middle) Controlled potential E_{x_t} at several times during the erasure protocol. (Bottom) Representative behavior via 1000 microstate trajectories in gray which sketches a profile of μ_t . A particular microstate trajectory $s_{0:\tau}$ is highlighted in red. (Note that $q_{0:\tau}$, shown explicitly, implies $\varphi_{0:\tau}$ by differentiation and so also implies $s_{0:\tau}$.)

To focus on computing we consider the channel $\Gamma_{s_{0:\tau}, x_{0:\tau} \rightarrow mm'} = \delta_{s_0 \in m} \delta_{s_\tau \in m'}$ which maps microstate trajectories to an observable that only tracks the initial and final memory states, such that the observable is a 2-tuple:

$$\vec{Y} = (\mathcal{M}_0, \mathcal{M}_\tau) .$$

For a particular realization $\mathcal{M}_0 = m$ and $\mathcal{M}_\tau = m'$, the time-reversal of the initial and final memory states is: $\mathbf{J}(m, m') = (m'^\dagger, m^\dagger)$, where $m^\dagger \equiv \{s^\dagger : s \in m\}$. This leads to observable memory transitions:

$$\begin{aligned} \rho((\mathcal{M}_0, \mathcal{M}_\tau) = (m, m')) \\ = \Pr_{x_{0:\tau}}(\mathcal{M}_0 = m, \mathcal{M}_\tau = m' | \mathcal{S}_0 \sim \mu_0) \end{aligned} \quad (7)$$

and the reversal probabilities:

$$\begin{aligned} \rho^R((\mathcal{M}_0, \mathcal{M}_\tau) = (m, m')) \\ = \Pr_{\mathbf{J}(x_{0:\tau})}(\mathcal{M}_0 = m'^\dagger, \mathcal{M}_\tau = m^\dagger | \mathcal{S}_0 \sim \mu_\tau^\dagger) . \end{aligned} \quad (8)$$

Appendix B uses this trajectory coarse-graining to show that the dissipated work is lower-bounded by a function

of the net transition probabilities between memory states:

$$\beta \langle W_{\text{diss}} \rangle = D_{\text{KL}} [\rho(\mathcal{S}_{0:\tau}) \parallel \rho^R(\mathcal{S}_{0:\tau})] \quad (9)$$

$$\geq D_{\text{KL}} [\rho(\mathcal{M}_0, \mathcal{M}_\tau) \parallel \rho^R(\mathcal{M}_0, \mathcal{M}_\tau)] \quad (10)$$

$$= \Delta H(\mathcal{M}_t) + \sum_{m, m' \in \mathcal{M}} \mu_0(m) d(m, m'), \quad (11)$$

where μ_t is the same preparation-and-driving-induced probability measure as previously introduced, such that $\mu_t(m) = \Pr(\mathcal{M}_t = m | \mathcal{S}_t \sim \mu_t) = \sum_{s \in m} \mu_t(s)$, and:

$$\Delta H(\mathcal{M}_t) = \sum_{m \in \mathcal{M}} \left(\mu_0(m) \ln \mu_0(m) - \mu_\tau(m) \ln \mu_\tau(m) \right)$$

is the change in Shannon entropy (in nats) of the coarse-grained memory states.

Note that Eq. (11) defined:

$$d(m, m') \equiv \Pr_{x_{0:\tau}}(\mathcal{M}_\tau = m' | \mathcal{S}_0 \sim \mu_0^{(m)}) \times \ln \left(\frac{\Pr_{x_{0:\tau}}(\mathcal{M}_\tau = m' | \mathcal{S}_0 \sim \mu_0^{(m)})}{\Pr_{\mathbf{H}(x_{0:\tau})}(\mathcal{M}_\tau = m' | \mathcal{S}_0 \sim \mu_\tau^{\dagger(m')})} \right), \quad (12)$$

where $\mu_t^{(m)} \equiv \delta_{\mathcal{S}_t \in m} \mu_t / \mu_t(m)$ is the renormalized microstate distribution μ_t restricted to memory m 's microstates. This compares (i) the probability of transitioning from memory state m to m' to (ii) the probability of returning to m^\dagger upon subsequent momentum-conjugation of the microstate distribution in m' and reversal of the control protocol. One concludes that dissipation is due to statistical irreversibility. At first sight, Eqs. (11) and (12) do not appear to significantly simplify the problem of inferring dissipation from partial knowledge. However, the practical constraints of reliable computation greatly simplify $d(m, m')$, as we will see shortly.

To emphasize, written as either Eq. (10) or (11), the bound applies when the conjugate $m^\dagger \equiv \{s^\dagger : s \in m\}$ of a memory state m is an element of the memory partition, $m^\dagger \in \mathcal{M}$, for all m . (However, see App. B for the more general case.) This occurs, for example, when spatial cells store a memory that is indifferent to rapidly fluctuating momentum degrees of freedom, so that $m = m^\dagger$. A similar simplification occurs for magnetic memory where s and s^\dagger are always in different memory states, such that $m^\dagger \in \mathcal{M}$ although $m \neq m^\dagger$. These two types of memory, illustrated in Fig. 3, lead to notable physical consequences; ones that we explore in a sequel.

C. Metastable Processing

Further simplifying Eq. (11)'s bound on dissipated work turns on recognizing a common property of informa-

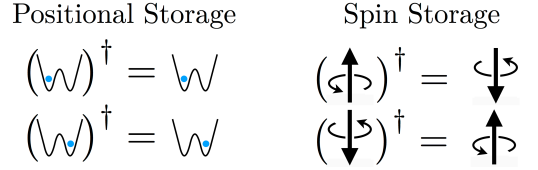


FIG. 3. Common memory elements are either time-reversal invariant (where $m^\dagger = m$) or flip under time-reversal (such that $m^\dagger \neq m$ although $m^\dagger \in \mathcal{M}$).

tion processing systems: They hold memory states as metastable nonequilibrium distributions. This has profound thermodynamic implications.

The implied timescale separation means that relaxing to the local-equilibrium distribution $\pi_x^{(m)}$ within each memory region is fast, while relaxing to the global equilibrium distribution π_x is much slower than the timescale of (and between) a system's computational steps. On the one hand, *metastable distributions* are those that correspond (up to some approximation) to a normalized weighted sum of local-equilibrium distributions. On the other, the *global equilibrium distribution* corresponding to any x is the canonical one: $\pi_x(s) = e^{-\beta E_x(s)} / \sum_{s' \in \mathcal{S}} e^{-\beta E_x(s')}$. The system approaches it in the limit of infinite time, if the control setting x is held fixed. In this, the *local-equilibrium distributions* $\pi_x^{(m)}(s) = \delta_{s \in m} \pi_x(s) / \sum_{s' \in m} \pi_x(s')$ are the canonical distributions, associated with each nearly-autonomous region of state space, that local densities approach much more quickly due to timescale separation [25].

If metastable memories are stored robustly between computations, then the memory-state distribution $\mu_t(m)$ at times $t = 0$ and $t = \tau$ contain almost all the information about the microstate distributions at the start and end times; or, at least, at the beginning and shortly *after* the end time. Indeed, the local distributions associated with each memory state are then nearly local-equilibrium distributions. If, to the contrary, the ending microstate distribution $\mu_\tau(s)$ is *not* yet metastable, then it quickly *relaxes* to the metastable distribution $\mu_{\tau+\delta t}(s) \approx \sum_{m \in \mathcal{M}} \mu_\tau(m) \pi_{x_\tau}^{(m)}(s)$. This results in yet more dissipation.

To include all dissipation associated with a computation, we extend a given protocol's start and end times to include most of the post-computation relaxation to metastability. Assuming a metastable distribution at the beginning and end of the computation means $\mu_0^{(m)} \approx \pi_{x_0}^{(m)}$ and $\mu_\tau^{(m)} \approx \pi_{x_\tau}^{(m)}$ and the full microstate distributions are then $\mu_0 \approx \sum_{m \in \mathcal{M}} \mu_0(m) \pi_{x_0}^{(m)}$ and $\mu_\tau \approx \sum_{m \in \mathcal{M}} \mu_\tau(m) \pi_{x_\tau}^{(m)}$, respectively. Thus, the beginning and ending microstate distributions are almost entirely determined by the distribution over memory states.

Initial and final memory-system metastability means that the empirically-observable memory transitions are always implicitly conditioned on metastability:

$$\begin{aligned} \Pr_{x_{0:\tau}}(\mathcal{M}_\tau = m' | \mathcal{M}_0 = m) \\ = \Pr_{x_{0:\tau}}(\mathcal{M}_\tau = m' | \mathcal{M}_0 = m, \mathcal{S}_0 \sim \pi_{x_0}^{(m)}) . \end{aligned}$$

Similarly, if we operate the control protocol in reverse, starting metastably under the influence of x_τ^\dagger , the observed memory-transition probabilities are:

$$\begin{aligned} \Pr_{\mathbf{A}(x_{0:\tau})}(\mathcal{M}_\tau = m^\dagger | \mathcal{M}_0 = m'^\dagger) \\ = \Pr_{\mathbf{A}(x_{0:\tau})}(\mathcal{M}_\tau = m^\dagger | \mathcal{M}_0 = m'^\dagger, \mathcal{S}_0 \sim \pi_{x_\tau^\dagger}^{(m'^\dagger)}) . \end{aligned} \quad (13)$$

Note, for comparison with Eq. (12), that:⁶

$$\pi_x^\dagger(s) = \pi_x(s^\dagger) = \pi_{x^\dagger}(s) .$$

And so, we have:

$$\pi_{x_\tau^\dagger}^{(m'^\dagger)} = \pi_{x_\tau}^{(m'^\dagger)} = \mu_\tau^{(m'^\dagger)} .$$

This allows us to remove all dependence on microstates from the work bound and estimate dissipation purely from observed memory-state trajectories. In particular, Eq. (12) simplifies to:

$$\begin{aligned} d(m, m') = \Pr_{x_{0:\tau}}(\mathcal{M}_\tau = m' | \mathcal{M}_0 = m) \\ \times \ln \frac{\Pr_{x_{0:\tau}}(\mathcal{M}_\tau = m' | \mathcal{M}_0 = m)}{\Pr_{\mathbf{A}(x_{0:\tau})}(\mathcal{M}_\tau = m^\dagger | \mathcal{M}_0 = m'^\dagger)} . \end{aligned} \quad (14)$$

Now, the dissipated work bound can be expressed in terms only of the probabilities of memory-state inputs and outputs:

$$\begin{aligned} \beta \langle W_{\text{diss}} \rangle \geq \Delta H(\mathcal{M}_t) + \sum_{m, m'} \Pr_{x_{0:\tau}}(\mathcal{M}_\tau = m', \mathcal{M}_0 = m) \\ \times \ln \frac{\Pr_{x_{0:\tau}}(\mathcal{M}_\tau = m' | \mathcal{M}_0 = m)}{\Pr_{\mathbf{A}(x_{0:\tau})}(\mathcal{M}_\tau = m^\dagger | \mathcal{M}_0 = m'^\dagger)} . \end{aligned}$$

This bounds a computation's dissipated energy using only knowledge of the memory-state transitions that result from forward driving $x_{0:\tau}$ and reverse driving $\mathbf{A}(x_{0:\tau})$. However, additional simplifications arise, if the driving is time-symmetric.

D. Time Symmetric Driving

Let us now consider the consequences for reliable computing with *time-symmetric* protocols—those for which $x_{0:\tau} = \mathbf{A}(x_{0:\tau})$ —as shown in the upper panel of Fig. 2's computation. In these cases, Eq. (14) simplifies considerably:

$$\begin{aligned} d(m, m') = \Pr_{x_{0:\tau}}(\mathcal{M}_\tau = m' | \mathcal{M}_0 = m) \\ \times \ln \left(\frac{\Pr_{x_{0:\tau}}(\mathcal{M}_\tau = m' | \mathcal{M}_0 = m)}{\Pr_{x_{0:\tau}}(\mathcal{M}_\tau = m^\dagger | \mathcal{M}_0 = m'^\dagger)} \right) . \end{aligned} \quad (15)$$

With Eqs. (11) and (15), we arrive at the remarkable result that the minimal dissipation depends only on memory-transition probabilities actually exercised by the computation:

$$d(m, m') = p(m \rightarrow m') \ln \frac{p(m \rightarrow m')}{p(m'^\dagger \rightarrow m^\dagger)} ,$$

where we rewrote the result suggestively denoting the computation as $p(m \rightarrow m') = \Pr_{x_{0:\tau}}(\mathcal{M}_\tau = m' | \mathcal{M}_0 = m)$. (Conveniently, no longer is there a dependence on counterfactual probabilities that *would* be induced by time-reversed driving.) Thus, the bound on dissipated work $\langle W_{\text{diss}} \rangle_{\min}^{t\text{-sym}}$ includes a term $\Delta H(\mathcal{M})$ that depends on initial and final observable distributions and one that depends on the transition paths between memory states:

$$\begin{aligned} \beta \langle W_{\text{diss}} \rangle_{\min}^{t\text{-sym}} = \Delta H(\mathcal{M}_t) \\ + \sum_{m, m'} \mu_0(m) p(m \rightarrow m') \ln \frac{p(m \rightarrow m')}{p(m'^\dagger \rightarrow m^\dagger)} . \end{aligned} \quad (16)$$

This demonstrates how restricting to time-symmetric control leads to unavoidable dissipation that depends explicitly on a computation's logic.

This adds to a short list of work bounds determined by the computation implemented. Original on this list—the minimal work required for a computation without control restrictions—is simply Landauer's bound:

$$\langle W \rangle_{\min}^{\text{Landauer}} \equiv -k_B T \Delta H(\mathcal{M}_t) ,$$

when memory states all have equal local free energies. More generally, though, as seen from Eq. (3), the minimal work required for a computation is:

$$\langle W \rangle_{\min} \equiv \Delta \mathcal{F} \quad (17)$$

$$= \Delta \langle F_{x_t}^{(\mathcal{M}_t)} \rangle + \langle W \rangle_{\min}^{\text{Landauer}} , \quad (18)$$

which is achieved in the limit of zero dissipation. Here, we recalled that for metastable distributions the nonequi-

⁶ That $(\pi_x)^\dagger = \pi_{x^\dagger}$ follows from the energy eigenvalues being invariant under time reversal: $E_x(s) = E_{x^\dagger}(s^\dagger)$. Note that equilibrium probability depends only on the energy of the state and on the partition function. $E_x(s) = E_{x^\dagger}(s^\dagger)$ implies $Z_x = Z_{x^\dagger}$. These properties together therefore imply $(\pi_x)^\dagger = \pi_{x^\dagger}$.

librium free energy decomposes as:

$$\mathcal{F} = \langle F_{x_t}^{(\mathcal{M}_t)} \rangle - k_B T H(\mathcal{M}_t) ,$$

where $F_x^{(m)} \equiv -k_B T \ln(\sum_{s \in m} e^{-\beta E_x(s)})$ is the local-equilibrium free energy associated with the memory m [5, 26].

Another, important but often overlooked result emerges.

Even for logically-irreversible computations, the minimal work required by this generalized Landauer bound is *reversible*: it corresponds to a stored change in nonequilibrium free energy. Thus, no work needs to be dissipated. We *could* have $\langle W_{\text{diss}} \rangle = 0$ in the case of unrestricted control. And, this alerts us to additional opportunities for optimizing implementations.

Appealing to Eq. (3) again, we see that the minimum total work under time-symmetric driving must be:⁷

$$\begin{aligned} \langle W \rangle_{\min}^{t\text{-sym}} &= \Delta \langle F_{x_t}^{(\mathcal{M}_t)} \rangle + \langle W \rangle_{\min}^{\text{Landauer}} + \langle W_{\text{diss}} \rangle_{\min}^{t\text{-sym}} \\ &= \Delta \langle F_{x_t}^{(\mathcal{M}_t)} \rangle + k_B T \sum_{m, m'} \mu_0(m) p(m \rightarrow m') \ln \frac{p(m \rightarrow m')}{p(m^\dagger \rightarrow m^\dagger)} . \end{aligned} \quad (19)$$

The consequences are immediate. Computing with time-symmetric protocols requires additional work above and beyond the Landauer bound. Moreover, all of this work—beside the reversible Landauer contribution and the change in local free energy—must be irreversibly dissipated since it is not stored as nonequilibrium free energy. $\langle W_{\text{diss}} \rangle > 0$, quantified precisely by Eq. (16), contributes to wasted heat in any computer. It adds on top of other beyond-Landauer work bounds including (i) the cost of modular computations, where global correlations are dissipated due to localized control [5, 33] and (ii) the cost of neglecting the local statistics of the manipulated memory [5, 34].

E. (Non)Reciprocity

We argued that it is common—in practice and, occasionally, out of necessity—for a computation to be implemented by transforming metastable memories with time-symmetric driving. We are now in a position to plainly state the thermodynamic consequences of this type of computation.

Generically, a physical computation produces and is characterized by the set of memory transition probabilities: $\{p(m \rightarrow m')\}_{m, m' \in \mathcal{M}}$. From Eq. (19), we see that the work required for such a computation, beyond the change

in local free energy (which is often constructed to be zero), is determined by the *nonreciprocity* of memory transitions. We say that a memory transition is *reciprocated* if:

$$p(m \rightarrow m') = p(m'^\dagger \rightarrow m^\dagger) . \quad (20)$$

Nonreciprocity Ψ quantifies the deviation from this:

$$\Psi(m \rightarrow m') \equiv \ln \frac{p(m \rightarrow m')}{p(m'^\dagger \rightarrow m^\dagger)} . \quad (21)$$

Notably, it vanishes when Eq. (20) is satisfied. Keep in mind that m^\dagger and m'^\dagger are themselves valid memory states, so nonreciprocity compares the probability of two different memory transitions.

Appendix C establishes the transition-specific version of Eq. (19). To summarize, we first derive a useful transition-specific fluctuation theorem:

$$\begin{aligned} \langle e^{-\beta W} \rangle_{\text{Pr}_{x_0:\tau}(\mathcal{S}_{0:\tau} | \mathcal{M}_\tau = m', \mathcal{S}_0 \sim \pi_{x_0}^{(m)})} \\ = e^{-\beta \Delta F_x^{(\mathcal{M})}} \frac{\text{Pr}_{\mathbf{R}(x_0:\tau)}(\mathcal{M}_\tau = m^\dagger | \mathcal{S}_0 \sim \pi_{x_\tau}^{(m'^\dagger)})}{\text{Pr}_{x_0:\tau}(\mathcal{M}_\tau = m' | \mathcal{S}_0 \sim \pi_{x_0}^{(m)})} , \end{aligned} \quad (22)$$

which applies to systems that start in local equilibrium. The appearance of the local-equilibrium free energies makes this a useful generalization of related past results [35]. By Jensen's inequality, and assuming time-symmetric control, this then implies that the minimal average work required of a memory transition is:

$$\begin{aligned} W_{\min}^{t\text{-sym}}(m \rightarrow m') \\ = F_{x_0}^{(m')} - F_{x_0}^{(m)} + k_B T \Psi(m \rightarrow m') . \end{aligned} \quad (23)$$

⁷ Common computational substrates have $\Delta \langle F_{x_t}^{(m)} \rangle = 0$, since engineered memories typically have equal local-equilibrium energies. The change in local free energy is nevertheless likely important in the manipulation of biological memories.

In the common scenario where all local-equilibrium free energies are constructed to be equal, this reduces to:

$$W_{\min}^{t\text{-sym}}(m \rightarrow m') = k_B T \Psi(m \rightarrow m') . \quad (24)$$

In other words, *nonreciprocity implies work*. This can also be seen from *Trajectory Class Fluctuation Theorems* if one restricts to trajectories that start and end in the specified memory states [36]. Not all work is bad, though. When $W_{\min}^{t\text{-sym}}(m \rightarrow m')$ is negative, some work can be harvested during the transition. In fact, such work harvesting is necessary to achieve minimal dissipation.

Equation (24) implies that *strictly reciprocal* computations, for which Eq. (20) is satisfied for all $m, m' \in \mathcal{M}$, can be implemented with a time-symmetric protocol with no expended work at all. The identity map is a trivial example. Two-cycles, like a bit swap, can also be implemented for free if using a time-symmetric memory substrate (for which $m^\dagger = m$ for all $m \in \mathcal{M}$). However, most computations require nonreciprocated memory transitions and, so, require work.

While the Landauer work cost corresponds to average state-space compression, nonreciprocity corresponds to a localized imbalance of memory currents. Even in the case of heterogeneous local free energies (i.e., Eq. (23)), the minimal dissipation required of time-symmetrically driven computations is the difference between the two:

$$\langle W_{\text{diss}} \rangle_{\min}^{t\text{-sym}} = k_B T \langle \Psi(\mathcal{M}_0 \rightarrow \mathcal{M}_\tau) \rangle - \langle W \rangle_{\min}^{\text{Landauer}} . \quad (25)$$

The expected nonreciprocity $\langle \Psi(\mathcal{M}_0 \rightarrow \mathcal{M}_\tau) \rangle$ weights how often a nonreciprocated transition is exercised. This uses the *weighted nonreciprocity* $d(m \rightarrow m')$:

$$d(m \rightarrow m') = p(m \rightarrow m') \Psi(m \rightarrow m') , \quad (26)$$

which appeared previously in Eq. (15). The nonreciprocity weight is critical to the following analysis. Though $\Psi(m \rightarrow m') = -\Psi(m'^\dagger \rightarrow m^\dagger)$, weighted nonreciprocity can strongly break the symmetry.

Consider a typical computation that enforces logical transitions: some transitions should happen with certainty while others should be forbidden. In particular, consider a nonreciprocated $m \mapsto m'$ logical transition: $m \mapsto m'$ should be strongly enforced ($p(m \rightarrow m') \approx 1$), while $m'^\dagger \not\mapsto m^\dagger$ should be strongly forbidden ($p(m'^\dagger \rightarrow m^\dagger) < \epsilon \ll 1$ for some error tolerance $\epsilon \rightarrow 0$). Then $d(m \rightarrow m')$ diverges as $\ln(1/\epsilon)$ while $d(m'^\dagger \rightarrow m^\dagger)$ vanishes. In short, divergent work is required to implement the desired nonreciprocated $m \mapsto m'$ logical transition.

A *deterministic* computation \mathcal{C} imparts a deterministic logical transformation $m \mapsto \mathcal{C}(m)$ satisfying the reciprocity

condition of Eq. (20) only when:

$$\mathcal{C}(\mathcal{C}(m)^\dagger)^\dagger = m . \quad (27)$$

If Eq. (27) is *not* satisfied—i.e., if $\mathcal{C}(m) = m'$ but $\mathcal{C}(m'^\dagger) \neq m^\dagger$ —then the logical transformation appears to require *infinite* work and *infinite* dissipation since, from Eq. (19), it appears to require work of $k_B T \ln \frac{1}{0}$. In practice, since dissipation is bounded, such logical transformations can only be approximated. Reliable logic (with a probability of error less than some small ϵ) requires significant dissipation of at least $k_B T \ln(1/\epsilon)$ for each violation of Eq. (27). Section III develops the consequences of this new relationship between reliability and dissipation. That then allows us to explore how the two can be balanced in several examples.

F. Time Symmetric Memory

The following explores the implications of these results for time-reversal-invariant memories— $m = m^\dagger$ —in which information is stored via time-symmetric variables, such as spatial location or physical conformation. In these cases, Eq. (16) simplifies to:

$$\begin{aligned} \beta \langle W_{\text{diss}} \rangle_{\min}^{t\text{-sym}} &= \Delta H(\mathcal{M}_t) + \sum_{m, m'} \mu_0(m) p(m \rightarrow m') \ln \frac{p(m \rightarrow m')}{p(m' \rightarrow m)} . \end{aligned} \quad (28)$$

As before, minimal dissipation depends directly on the nonreciprocity between memory transitions, but now we have the simplification that:

$$\Psi(m \rightarrow m') = \ln \frac{p(m \rightarrow m')}{p(m' \rightarrow m)} .$$

And here, reciprocity has an especially straightforward interpretation: If m maps to m' , then m' should map back to m with the same probability. Otherwise work is required and, if it is above the Landauer bound, it must be dissipated.

What is reciprocity in the limit of deterministic computation? For time-symmetric memory, it acts somewhat like logical invertibility. However, it is stricter. Rather, it is logical self-invertibility. Logical noninvertibility, in contrast, gives rise to state-space compression—the origin of the Landauer bound. Indeed, circumventing the latter led early researchers to investigate *reversible* computing—computing with invertible logical transformations [1]. Logically reversible computing requires no work to operate. However, it is now understood that even logically irre-

versible computing can be accomplished with zero dissipation, despite requiring some recyclable work [2–4].

The next section draws out the consequences of nonreciprocity in the limit of nearly deterministic computation. In contrast to the Landauer cost of logical irreversibility—which, in the limit of zero error, saturates to some small value on the order of the thermal energy—the thermodynamic cost of nonreciprocity *diverges* in the limit of zero error, with no chance of recovering the input energy. It demands an accounting.

III. ALMOST-DETERMINISTIC COMPUTING

At this point, we showed that the transition probabilities entailed by a desired logical transformation set a lower bound on the work required to instantiate it physically. We noted that this gives a much stronger bound than that due to Landauer, which only depends on the relative state-space volume supporting memory before and after a computation. More specifically, when time-symmetric control implements a transformation of metastable memories, the minimal work investment is proportional to the reciprocity (self-invertibility) of memory transitions. Furthermore, we discovered that the time-reversal symmetries of the memory elements themselves can substantially alter the minimal thermodynamic costs.

Drawing out the practical consequences, the following shows that computing with minimum work by minimizing nonreciprocity depends directly on a computation's error rate ϵ . Most concretely, time-symmetry-induced dissipation diverges as $\ln(1/\epsilon)$ for almost-deterministic computation, where metastable memories are transformed at low error rate $\epsilon \rightarrow 0$.

Consider the physical memory apparatus of a computer that approximately implements a deterministic computation $\mathcal{C}: \mathcal{M} \rightarrow \mathcal{M}$, mapping memory states to memory states. Then, the memory-state transition probabilities appearing in Eq. (16) are strongly constrained by the computation's desired reliability. That is, the probability that the nonequilibrium thermodynamic information processing takes a memory state m to anywhere besides $\mathcal{C}(m)$ must be no greater than the error tolerance ϵ , with $0 < \epsilon \ll 1$. Reliability requires choosing a time-symmetric drive protocol $x_{0:\tau}$ that guarantees that $\Pr_{x_{0:\tau}}(\mathcal{M}_\tau = m' | \mathcal{M}_0 = m) \leq \epsilon$ for all $m, m' \in \mathcal{M}$ such that $m' \neq \mathcal{C}(m)$. The thermodynamic implications for a reliable computation then follow from Eq. (16) with:

$$p(m \rightarrow m') \begin{cases} \geq 1 - \epsilon & \text{if } \mathcal{C}(m) = m' \\ \leq \epsilon & \text{if } \mathcal{C}(m) \neq m' \end{cases}.$$

Evaluating Eq. (16) requires addressing four cases, depending on whether $\mathcal{C}(m) = m'$ or $\mathcal{C}(m) \neq m'$ and on whether $\mathcal{C}(m^\dagger) = m^\dagger$ or $\mathcal{C}(m^\dagger) \neq m^\dagger$. Any given implementation results in an *actual* probability of error for each of the intended transitions: $\epsilon_m = 1 - p(m \rightarrow \mathcal{C}(m))$. We adopt the design constraint that $\epsilon_m \leq \epsilon$ for all possible initial memories m . Then, given an implementation $x_{0:\tau}$, the probability of an *accidental* memory transition is $\epsilon_{m \rightarrow m'} = p(m \rightarrow m')$ for $m' \neq \mathcal{C}(m)$. Since $\sum_{m' \in \mathcal{M} \setminus \{\mathcal{C}(m)\}} \epsilon_{m \rightarrow m'} = \epsilon_m \leq \epsilon$, we must have that $0 < \epsilon_{m,m'} \leq \epsilon_m \leq \epsilon$.

To simplify, we temporarily restrict to the case of time-reversible memories, where $m = m^\dagger$. There are then four cases to consider when evaluating Eq. (28), depending on whether $\mathcal{C}(m) = m'$ or $\mathcal{C}(m) \neq m'$, and on whether $\mathcal{C}(m') = m$ or $\mathcal{C}(m') \neq m$. Later, we quote the general result that does not require $m = m^\dagger$.

Appendix D uses the error constraints to evaluate the weighted nonreciprocity:

$$d(m, m') = p(m \rightarrow m') \ln \frac{p(m \rightarrow m')}{p(m' \rightarrow m)},$$

for the four possible cases, finding:

1. $\mathcal{C}(m) = m'; \mathcal{C}(m') = m$:
 $-\epsilon \leq d^{(1)}(m, m') \leq \epsilon + \frac{1}{2}\epsilon^2 + \mathcal{O}(\epsilon^3)$.
2. $\mathcal{C}(m) = m'; \mathcal{C}(m') \neq m$:
 $\ln(\epsilon^{-1}) \lesssim d^{(2)}(m, m') \leq \ln(\epsilon_{m' \rightarrow m}^{-1})$.
3. $\mathcal{C}(m) \neq m'; \mathcal{C}(m') = m$:
 $\epsilon_{m \rightarrow m'} \ln \epsilon_{m \rightarrow m'} < d^{(3)}(m, m') < 0$.
4. $\mathcal{C}(m) \neq m'; \mathcal{C}(m') \neq m$:
 $d^{(4)}(m, m') = \epsilon_{m \rightarrow m'} \ln \left(\frac{\epsilon_{m \rightarrow m'}}{\epsilon_{m' \rightarrow m}} \right)$.

In the high-reliability limit $\epsilon \rightarrow 0$, most $d^{(n)}(m, m')$ terms are on the order of ϵ and so tend to zero. That is, *except* for $d^{(2)}(m, m')$ in Case 2 whose contribution to the dissipation *diverges* as $\epsilon \rightarrow 0$ since $d^{(2)}(m, m') \gtrsim \ln(\epsilon^{-1})$.

Case 4 is somewhat more delicate than Cases 1 and 3, due to the ratio of errors. When $\epsilon_{m' \rightarrow m} \geq \epsilon_{m \rightarrow m'}$, then $-\epsilon/\epsilon \leq d^{(4)}(m, m') \leq 0$, so that $d^{(4)}(m, m')$ vanishes as $\epsilon \rightarrow 0$. However, when $\epsilon_{m \rightarrow m'} > \epsilon_{m' \rightarrow m}$, there is a chance for slightly more dissipation. Nevertheless, $d^{(4)}(m, m')$ is still only on the order of ϵ , so long as the relative error rates $\epsilon_{m \rightarrow m'}$ and $\epsilon_{m' \rightarrow m}$ are within several orders of magnitude of each other. If $\epsilon_{m \rightarrow m'} \gg \epsilon_{m' \rightarrow m}$, then extra dissipation will be incurred due to the stringent reliability of the forbidden $m \rightarrow m'$ transition, beyond the design constraint.

The upper bound in Case 2 also implies extra dissipation when $\epsilon_{m' \rightarrow m}$ is more reliable than the reliability design constraint. And, this extra dissipation need not be small.

Generically, though, for a given error tolerance, we expect that minimal dissipation can be achieved by allowing all error rates to be as close to uniform as possible, meeting but not significantly exceeding the overall reliability constraint. Still, due to Case 2, even the minimal dissipation diverges with increasing reliability.

Thus, Case 2 provides the only contribution of the $d(m, m')$ terms to Eq. (11) in the low-error limit. Since the target computation is deterministic— \mathcal{C} maps each memory state m to one memory state $\mathcal{C}(m)$ —there can be at most one contribution of $d^{(2)}(m, m')$ for each m , coming from $m' = \mathcal{C}(m)$, and only if $\mathcal{C}(m') \neq m$. The total contribution from each m is:

$$[\mathcal{C}(\mathcal{C}(m)) \neq m] \ln(\epsilon_{\mathcal{C}(m) \rightarrow m}^{-1}),$$

where $[\cdot]$ is the Iverson bracket, which returns 1 when its argument is true and 0 otherwise. In this case, $[\mathcal{C}(\mathcal{C}(m)) \neq m] = 1 - \delta_{m, \mathcal{C}(\mathcal{C}(m))}$.

Applying the low- ϵ contributions to Eq. (15) yields an approximate bound for the time-symmetric work. If the memories have the same local-equilibrium free energy, the bound is:

$$\begin{aligned} \beta \langle W \rangle_{\min}^{t\text{-sym}} &\approx \sum_{m \in \mathcal{M}} \mu_0(m) [\mathcal{C}(\mathcal{C}(m)) \neq m] \ln(\epsilon_{\mathcal{C}(m) \rightarrow m}^{-1}) \\ &\geq \ln(\epsilon^{-1}) \sum_{m \in \mathcal{M}} \mu_0(m) [\mathcal{C}(\mathcal{C}(m)) \neq m] \\ &= \beta \langle W \rangle_{\min}^{\text{approx}}. \end{aligned} \quad (29)$$

This determines how the tradeoff between work and reliability scales for almost-perfect computation. And, it identifies the role that a computation's reciprocity plays in dissipation.

The result is a simple error–dissipation tradeoff, if we restrict ourselves to using time-reversible protocols for implementing reliable computations:

$$\begin{aligned} \beta \langle W_{\text{diss}} \rangle_{\min}^{t\text{-sym}} &\gtrsim \beta \langle W_{\text{diss}} \rangle_{\min}^{\text{approx}} \\ &= \langle [\mathcal{C}(\mathcal{C}(\mathcal{M}_0)) \neq \mathcal{M}_0] \rangle_{\mathcal{M}_0} \ln(\epsilon^{-1}) \\ &\quad + \Delta H(\mathcal{M}_t). \end{aligned} \quad (30)$$

Since the change $\Delta H(\mathcal{M}_t)$ in entropy is finite as $\epsilon \rightarrow 0$, the divergent nonreciprocity contribution to the dissipation dominates. Moreover, the simple scaling of the reliability–dissipation tradeoff is the same as that for the reliability–work tradeoff. In the low-error limit, the minimal nonreciprocity depends only on the computation:

$$\langle \Psi(\mathcal{M}_0 \rightarrow \mathcal{M}_\tau) \rangle \geq \langle [\mathcal{C}(\mathcal{C}(\mathcal{M}_0)) \neq \mathcal{M}_0] \rangle_{\mathcal{M}_0} \ln(\epsilon^{-1}).$$

The reciprocity coefficient:

$$\langle [\mathcal{C}(\mathcal{C}(\mathcal{M}_0)) \neq \mathcal{M}_0] \rangle_{\mathcal{M}_0} = \sum_{m \in \mathcal{M}} \mu_0(m) [\mathcal{C}(\mathcal{C}(m)) \neq m]$$

is the probability that the memory makes a transition that is *not* reciprocated if the output becomes the input to the computation. In short, *computations with nonreciprocity require significant dissipation when implemented with a time-symmetric protocol.*

A sequel explores the dynamical mechanism for the dissipation in this case. With time-symmetric protocols, state-space compression occurs only via a loss of stability and subsequent dissipation. This corresponds to a topological restriction on the bifurcation structure of local attractors—a restriction imposed by time-symmetric control.

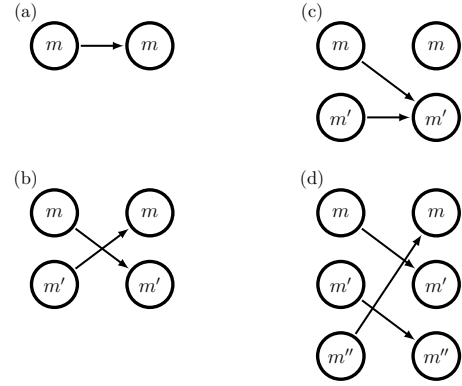


FIG. 4. Simple features of deterministic computations determine the minimal dissipation required to implement them reliably with time-symmetric protocols. Dissipation is incurred for nonreciprocated memory transitions. When using time-reversal-invariant memory elements ($m^\dagger = m$): (a) identity mappings and (b) swap operations can be implemented freely, whereas (c) memory-space compression and (d) nonreciprocated permutations require dissipation that diverges with increasing reliability.

One also concludes that strictly-reciprocal logic gates, such as the identity (communication relay) and NOT gates, where $\mathcal{C}(\mathcal{C}(m))$ always returns m , are *exempt* from this dissipation. One can efficiently implement them with time-symmetric protocols. For all other computations, time-*asymmetric* control must be used to avoid this dissipation. Figure 4 gives examples of reciprocated and nonreciprocated memory transitions.

The main result Eq. (29) generalizes to the case where $m, m^\dagger \in \mathcal{M}$ without the requirement that $m = m^\dagger$. Then, dissipation diverges with increasing reliability whenever $m \rightarrow m'$ transitions are made such that $\mathcal{C}(m) = m'$ but $\mathcal{C}(m'^\dagger) \neq m^\dagger$. For uniform local free energies, Eq. (29)

becomes:

$$\beta \langle W \rangle_{\min}^{\text{approx}} = \ln(\epsilon^{-1}) \sum_{m \in \mathcal{M}} \mu_0(m) [\mathcal{C}(\mathcal{C}(m)^\dagger) \neq m^\dagger]. \quad (31)$$

Notably, this allows one to quantify error–work and error–dissipation tradeoffs when computing with magnetic memory systems, for example. For a single bistable magnetic device, m could represent the **1** memory of having an “up” magnetic moment or “clockwise” in the case of toroidal magnetic core memory elements. And, m^\dagger would then represent the “down” or “counter-clockwise” memory **0**, as shown on the right side of Fig. 3. This implies that memories with certain types of symmetry are better suited for certain types of logical operation, in that they minimize nonreciprocity and so dissipation.

To emphasize, the dissipations here are distinct from the heat associated with logically-irreversible transformations, as discussed by Landauer and Bennett [1, 18], which arises as a compensation to microscopic state-space contraction. There are two important distinctions.

First, the heat devolved with logical irreversibility—e.g., the minimal heat of $k_B T \ln 2$ released to the environment upon erasure—is *not necessarily irreversibly dissipated* [2, 3, 5, 26]. It is offset by a change in the nonequilibrium addition to free energy and so can be leveraged later to do an equal amount of useful work.⁸ In contrast, nonreciprocity dissipation is energy that is truly dissipated. It is irretrievably lost to the environment, with no compensation via change of the nonequilibrium addition to free energy and so can never be recovered.

Second, logical nonreciprocity is distinct from logical irreversibility. Strictly-reciprocal computations, where $\mathcal{C}(\mathcal{C}(m)) = m$ for all $m \in \mathcal{M}$, are logically reversible, being their own inverses. However, logically reversible permutations of the memory can be completely nonreciprocal, as demonstrated in Fig. 4(d). Reciprocity requires not only that the deterministic logic be invertible, but further that the logical dynamic inverts itself. In short, the Landauer work cost corresponds to logical noninvertibility, while nonreciprocity cost corresponds to logical *noninvolution*. The reciprocity bound on dissipation can therefore be interpreted as the minimal work required to implement a reliable computation with time-symmetric protocols *in addition to* the well-known Landauer bound.

⁸ The modern understanding of the Landauer bound is that—when computing using memory states with equal local-equilibrium free energies—the minimal average work required for a computation is exactly opposite the change in the coarse-grained entropy of the memory: $\langle W \rangle_{\min} = -k_B T \Delta H(\mathcal{M}_t)$. Crucially, this work can be salvaged later and ultimately need *not* be dissipated.

IV. APPLICATIONS

With the basics of time-symmetric and nonreciprocal computing in hand, we turn to explore the thermodynamics of various erasure implementations, logic gates, and biological information processing.

A. Erasure

To illustrate how the cost of time-symmetric control differs from Landauer’s bound, consider the classic example of bit erasure. Landauer originally described a method for erasing a bit of information stored in a double-well potential in contact with a heat bath: tilt the potential—moving overdamped stochastic particles to one side—and return the potential to its original orientation, leaving the particles (temporarily) trapped in one well [18]. If implemented naively, via a protocol that raises the energy of one well and then lowers it at the same rate, the time-symmetry results in dissipation significantly above Landauer’s bound, as described by the bounds just developed. Note that protocol time-symmetry does *not* imply spatial symmetry—one can tilt the potential to the left without needing to tilt it to the right.

Bit erasure $\mathcal{C}_{\text{erase}}$ operates on a single bistable element with memory states $\mathcal{M} = \{L, R\}$ that correspond to occupying the Left or Right side of a double-well potential energy landscape. The computation is defined by resetting to the L memory state: $\mathcal{C}_{\text{erase}}(L) = L$ and $\mathcal{C}_{\text{erase}}(R) = L$. Hence, $\mathcal{C}_{\text{erase}}(\mathcal{C}_{\text{erase}}(L)) = L$, while $\mathcal{C}_{\text{erase}}(\mathcal{C}_{\text{erase}}(R)) \neq R$. Thus, the net transition probabilities $p(m \rightarrow m')$ shown in Fig. 5 characterize any reliable implementation of this computation in terms of the probabilities of errors, $\epsilon_R = \epsilon_{R \rightarrow R}$ and $\epsilon_L = \epsilon_{L \rightarrow R}$, that leave the system in the R state.

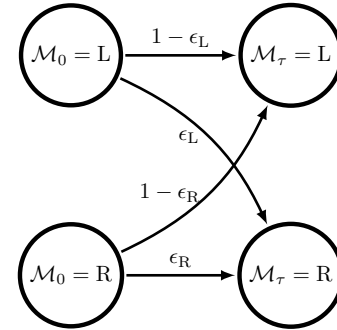


FIG. 5. Markov transition matrix for any implementation of erasure gives the error rate $\epsilon_L = \epsilon_{L \rightarrow R}$ from initial memory state $\mathcal{M}_0 = L$ and the error rate $\epsilon_R = \epsilon_{R \rightarrow R}$ from the initial memory state $\mathcal{M}_0 = R$.

From this, the only terms contributing to the bound on time-symmetric work are:

$$d(L, R) = \epsilon_L \ln \frac{\epsilon_L}{1 - \epsilon_R}$$

$$d(R, L) = (1 - \epsilon_R) \ln \frac{1 - \epsilon_R}{\epsilon_L}.$$

Allowing for a potentially nonuniform input distribution $\mu_0 = (1 - p_R, p_R)$ over memory states yields the exact bound on time-symmetric work investment:

$$\begin{aligned} \beta \langle W \rangle_{\min}^{t\text{-sym}} &= (1 - p_R) d(L, R) + p_R d(R, L) \\ &= (p_R(1 - \epsilon_R) - (1 - p_R)\epsilon_L) \ln \frac{1 - \epsilon_R}{\epsilon_L} \\ &= (p_R - \langle \epsilon \rangle) \ln \frac{1 - \epsilon_R}{\epsilon_L}, \end{aligned} \quad (32)$$

where $\langle \epsilon \rangle = p_R \epsilon_R + (1 - p_R) \epsilon_L$ is the average error of the computation.

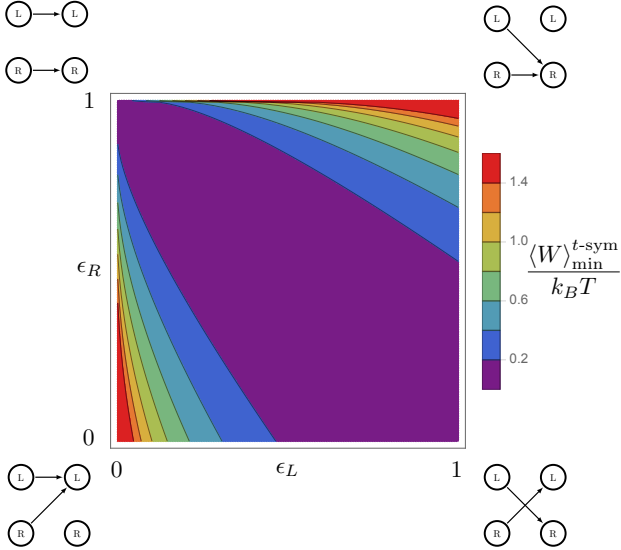


FIG. 6. Average minimum work (units of $k_B T$) required for a 1-bit operation diverges for low ϵ_L or high ϵ_R , corresponding to erasure to L or erasure to R, respectively. The state-transition diagrams at the corners show the basic computations associated with each extremal point in computation parameter space. The identity map (upper left), the bit-flip (lower right), and every operation interpolated between require no work according to the time-symmetric control bound. The required work diverges at perfect erasure to Left (bottom-left corner) and perfect erasure to Right (top-right corner), where the red coloring covers all work values from 1.4 to $\infty k_B T$.

Figure 6 plots the work requirements for an initially unbiased memory state with $p_R = 1/2$. We see that the error diverges for small values of error ϵ_L . The plot also indicates that the work diverges for high values of error

ϵ_R , due to the symmetry of the system between left and right. It is also worth noting from the plot that there are computations, such as bit flips, which this bound suggests may be achievable with time-symmetric control and without energetic cost. However, we are primarily concerned with the lower left portion of the plot, where effective erasures occur. The divergent scaling of the work required to reliably erase overwhelms the rather meager energy requirements given by Landauer's bound. And, unlike the latter, this excess work requirement must be irreversibly dissipated. Subtracting off the Landauer bound $k_B T \Delta H(\mathcal{M}_t)$ to calculate the minimum dissipation $\langle W_{\text{diss}} \rangle_{\min}^{t\text{-sym}}$, Fig. 7 shows that the divergent contribution to the work is attributed to nonreciprocity.

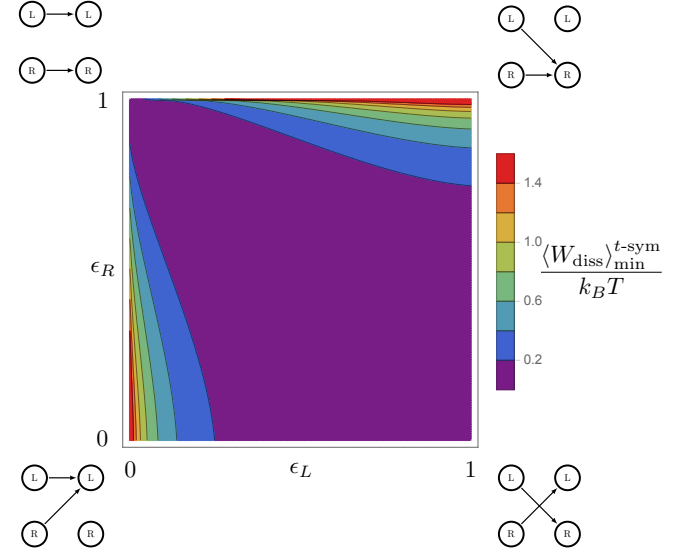


FIG. 7. Dissipated work above the Landauer bound: Similar to the minimum work over possible bit computations (Fig. 6), it too diverges for high values of ϵ_R and low values of ϵ_L and vanishes for the identity map and bit flip. Dissipation diverges at the bottom-left and top-right corners, where the red coloring covers all values of dissipated work from 1.4 to $\infty k_B T$.

Applying Eq. (29)'s work bounds to erasure, we see that:

$$\langle [\mathcal{C}_{\text{erase}}(\mathcal{C}_{\text{erase}}(\mathcal{M}_0)) \neq \mathcal{M}_0] \rangle_{\mathcal{M}_0} = p_R.$$

This means that, in the low-error limit:

$$\langle W \rangle_{\min}^{\text{approx}} = p_R \ln(\epsilon^{-1}) k_B T. \quad (33)$$

The initial memory-state entropy is $H_b(p_R) \equiv -p_R \ln p_R - (1 - p_R) \ln(1 - p_R) \leq \ln 2$ —the *binary entropy function*. Whereas, the final memory-state entropy vanishes as $\epsilon \rightarrow 0$. Hence, from Eq. (30), we immediately find that the small-error dissipation necessary for time-symmetric

erasure diverges as $\epsilon \rightarrow 0$:

$$\langle W_{\text{diss}} \rangle_{\text{min}}^{\text{approx}} \approx p_R \ln(\epsilon^{-1}) k_B T - H_b(p_R) k_B T. \quad (34)$$

Landauer erasure typically assumes a uniform initial distribution where $p_R = 1/2$. This results in $\langle W_{\text{diss}} \rangle^{t\text{-sym}} \gtrsim \frac{1}{2} \ln(1/4\epsilon) k_B T$. Since the memory-state entropy is bounded by $k_B T \ln 2$, the contribution from Landauer's bound is negligible compared to the $\ln(\epsilon^{-1})$ term for small ϵ . And so, the latter dominates both the work and dissipation for high-fidelity erasure. To test the strength of these bounds and their approximations, we consider two different implementations of time-symmetric erasure below—rate equations for a two-level system and one-dimensional Langevin dynamics in a controlled double-well potential.

1. Two-state rate equations

A direct test of time-symmetric erasure requires only a simple two-state system that evolves under a rate equation:

$$\begin{aligned} & \frac{d\text{Pr}(\mathcal{M}_t = m)}{dt} \\ &= \sum_{m'} [r_{m' \rightarrow m}(t) \text{Pr}(\mathcal{M}_t = m') - r_{m \rightarrow m'}(t) \text{Pr}(\mathcal{M}_t = m)], \end{aligned} \quad (35)$$

obeying the Arrhenius equations:

$$\begin{aligned} r_{R \rightarrow L}(t) &= A e^{-\Delta E_R(t)/k_B T} \text{ and} \\ r_{L \rightarrow R}(t) &= A e^{-\Delta E_L(t)/k_B T}, \end{aligned}$$

where the states are labeled $\{L, R\}$ and the terms $\Delta E_R(t)$ and $\Delta E_L(t)$ in the exponentials are the activation energies to transit over the energy barrier at time t for the Right and Left wells, respectively. These dynamics are a coarse-graining of thermal motion in a double-well potential energy landscape $V(q, t)$ over the positional variable q at time t . Above, A is an arbitrary constant, which is fixed for the dynamics. q_R^* and q_L^* are the locations of the Right and Left potential well minima, respectively. Thus, assuming that $q = 0$ is the location of the barrier's maximum between them, we see that the activation energies can be expressed as $\Delta E_R(t) = V(0, t) - V(q_R^*, t)$ and $\Delta E_L(t) = V(0, t) - V(q_L^*, t)$. By varying the potential energies, $V(q_R^*, t)$, and $V(q_L^*, t)$, at $V(0, t)$'s extrema we can control the dynamics of the observed variables $\{L, R\}$ in much the same way as is done with physical implementations of erasure where barrier height and tilt are controlled in a double-well [32].

Deviating from previous investigations of efficient erasure, where Landauer's bound was nearly achieved over long times [32, 37], here the constraint to symmetric driving

over the interval $t \in (0, \tau)$ results in additional dissipated work. As Landauer described [18], erasure can be implemented by turning on and off a tilt from R to L—a time symmetric protocol. However, to achieve higher fidelity, we also lower the barrier while the system is tilted energetically towards the L well.

Consider a family of control protocols that fit the profile shown in Fig. 8. First, we increase the energy tilt from R to L via the energy difference $V(q_R^*, t) - V(q_L^*, t)$ measured in units of $k_B T$. This increases the relative probability of transitioning R to L. However, with the energy barrier at it's maximum height, the transition takes quite some time. Thus, we reduce the energy barrier $V(0, t)$ to its minimum height halfway through the protocol $t = \tau/2$. Then, we reverse the protocol, raising the barrier back to its default height to hold the probability distribution fixed in the well and untilt so that the system resets to its default double-well potential.

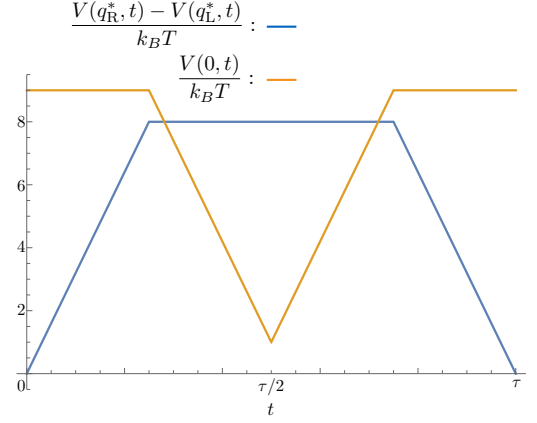


FIG. 8. Time-symmetric control protocol for implementing moderately-efficient erasure, compared to Landauer's original time-symmetric protocol. It starts by tilting—increasing the difference in potential energy $(V(q_R^*, t) - V(q_L^*, t))/k_B T$ between L and R. We increase this value such that transitions are more likely to go from R to L. Then we reduce the barrier height $V(0, t)$ to increase the total flow rate. Finally, we reverse the previous steps, cutting off the flow by raising the barrier, then untilting.

Increasing the maximum tilt—given by $V(q_R^*, \tau/2) - V(q_L^*, \tau/2)$ at the halfway time—increases erasure fidelity. Figure 9 shows that the maximum error $\epsilon = \max\{\epsilon_R, \epsilon_L\}$ decreases nearly exponentially with increased maximum energy difference between left and right, going below 1 error in every 1000 trials for our parameter range. Note that ϵ starts at a very high value (greater than 1/2) for zero tilt, since the probability $\epsilon_R = \epsilon$ of ending in the R well starting in the R well is very high if there is no tilt to push the system out of the R well.

Figure 9 also shows the relationship between the work and the bounds described above. Given that our system consists of two states $\{L, R\}$ and that we choose a control protocol which keeps the energy on the left $V(q_L^*, t)$ fixed, the work (marked by green +s in the figure) is [38]:

$$\begin{aligned} \langle W \rangle &= \int_0^\tau dt \sum_s \Pr(\mathcal{S}_t = s) \partial_t V(s, t) \\ &= \int_0^\tau dt \Pr(\mathcal{M}_t = R) \partial_t V(q_R^*, t). \end{aligned}$$

This work increases almost linearly as the error reduces exponentially.

As a first comparison, note that the Landauer bound $\langle W \rangle_{\min}^{\text{Landauer}} = -k_B T \Delta H(\mathcal{M}_t)$ (marked by orange x's in the figure) is still valid. However, it is a very weak bound for this time-symmetric protocol. The Landauer bound saturates at $k_B T \ln 2$. Thus, the dissipated work—the gap between orange x's and green +s—grows approximately linearly with increasing tilt energy.

In contrast, Eq. (32)'s bound $\langle W \rangle_{\min}^{t\text{-sym}}$ for time symmetric protocols is much tighter. The time symmetric bound is valid: marked by blue circles that all fall below the calculated work (green +s). Not only is this bound much stricter, but it almost exactly matches the calculated work for a large range of parameters, with the work only diverging for higher tilts and lower error rates.

Finally, the approximate bound $\langle W \rangle_{\min}^{\text{approx}} = \frac{k_B T}{2} \ln \epsilon^{-1}$ (marked by red +s), which captures the error scaling, behaves as expected. The error-dependent work bound nearly exactly matches the exact bound for low error rates on the right side of the plot and effectively bounds the work. For lower tilts, this quantity does not bound the work and is not a good estimate of the true bound, but this is consistent with expectations for high error rates. This approximation should only be employed for very reliable computations, for which it appears to be an excellent estimate. Thus, the two-level model of erasure demonstrates that the time-symmetric control bounds on work and dissipation are reasonable in both their exact and approximate forms at low error rates.

2. Underdamped double-well potential

The physics in the rate equations above represents a simple model of a bistable thermodynamic system, which can serve as an approximation for many different bistable systems. One possible interpretation is a coarse-graining of Langevin dynamics of a particle moving in a double-well potential. To explore the broader validity of the error–dissipation tradeoff, here we simulate the dynamics

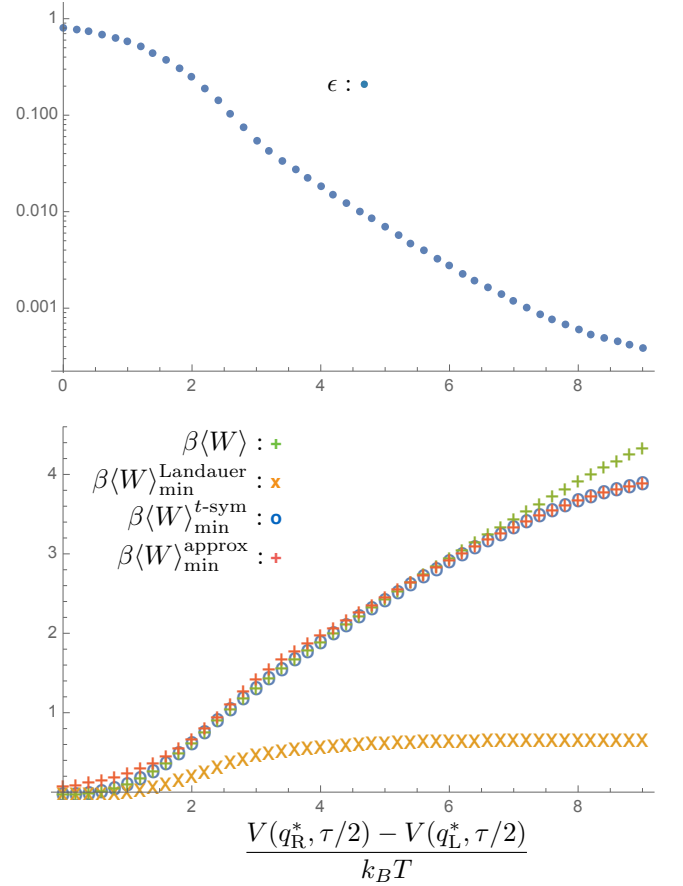


FIG. 9. (Top) Maximum error ϵ (blue dots) decreases approximately exponentially with increasing maximum tilt. The latter is given by the maximum energy difference between the right and left energy well $V(q_R^*, \tau/2) - V(q_L^*, \tau/2)$. (Bottom) Work $\langle W \rangle$ (green +s), scaled by the inverse temperature $\beta = 1/k_B T$, increases with increasing maximum tilt and decreasing error. The Landauer work bound $\langle W \rangle_{\min}^{\text{Landauer}}$ (orange x's) is a very weak bound, asymptoting to a constant value rather than continuing to increase, as the work does. The bound $\langle W \rangle_{\min}^{t\text{-sym}}$ (blue circles) on time-symmetrically driven protocols, on the other hand, is a very tight bound for lower values of maximum tilt. The work deviates from the time-symmetric bound for higher tilts. Finally, the approximate bound $\langle W \rangle_{\min}^{\text{approx}}$ (red +s), which scales as $\ln \epsilon^{-1}$, is not an accurate bound over the entire range, but it very closely matches the exact time-symmetric bound $\langle W \rangle_{\min}^{t\text{-sym}}$ for small ϵ , as expected.

of a stochastic particle coupled to a thermal environment at constant temperature and a work reservoir via a 1D potential. Appendix E gives the equations of motion and simulation methods. Again we find that our time-symmetric bounds are much tighter than Landauer's, reflecting the error–dissipation tradeoff of this control restriction.

We consider protocols that proceed similar to those shown in Fig. 8, but with additional passive substages: the first, middle and last substages hold the potential fixed while

the other four vary the potential smoothly in time: (i) hold the potential in the symmetric double-well form, (ii) positively tilt the potential, (iii) completely drop the potential barrier between the two wells, (iv) hold the potential while it is tilted with no barrier, (v) restore the original barrier, (vi) remove the positive tilt, restoring the original symmetric double-well, and (vii) hold the potential in this original form. For practical purposes, this gives the simulated distribution more time to relax to local-equilibrium within the current potential.

As described in Appendix E, the dynamics are parametrized by the relative amplitudes of temperature, damping, maximum barrier energy, and maximum tilt of the potential energy landscape. To explore the space of possible underdamped erasure dynamics, we simulated 735 different settings of these parameters, with 100,000 trials for each parameter setting. Figure 10 shows that the (error, work) pairs obtained for these various dynamics fill in the region allowed by our time-symmetric bounds. Our bounds can indeed be tight, but it is always possible to waste more energy if the computation is not tuned for energetic efficiency.

These underdamped simulations drive home the point that our bounds are independent of the details of the dynamics used for computation. Our results are very general in that regard. As long as the system *starts* metastable and is then driven by a time-symmetric protocol, the error-dissipation tradeoff quantifies the minimal dissipation that will be incurred (for a desired level of computational accuracy) by the time the system relaxes again to metastability.

As with erasure implemented in the two-state rate equation, we set $p_R = 1/2$, initializing the particle with equal probability to begin in the left and right wells. This leaves the exact work bound Eq. (32) with two degrees of freedom: ϵ_R and ϵ_L .

We compare the sampled average works obtained for each simulated protocol relative to the sampled maximum error $\epsilon = \max(\epsilon_L, \epsilon_R)$ and to the exact and approximate work bounds derived above. To do this, we shift the average works measured in the simulations as follows. We first take as a reference the exact work bound $\langle W \rangle_{\min}^{t\text{-sym}}$ from Eq. (32) as a function of ϵ for the case of $\epsilon_L = \epsilon_R = \epsilon$, referring to it here as $\langle W \rangle_{\text{ref}}^{t\text{-sym}}$ to highlight its role. Figure 10 plots it as a solid blue line. For each protocol, we then find the true bound $\langle W \rangle_{\min}^{t\text{-sym}}$ by substituting the sampled error rates ϵ_L and ϵ_R into Eq. (32). Then, we subtract this exact work bound from the reference bound at the corresponding ϵ . Adding this shift to the sampled average work $\langle W \rangle$ gives the shifted average work $\langle W \rangle_{\text{shift}}$ for a given simulated protocol.

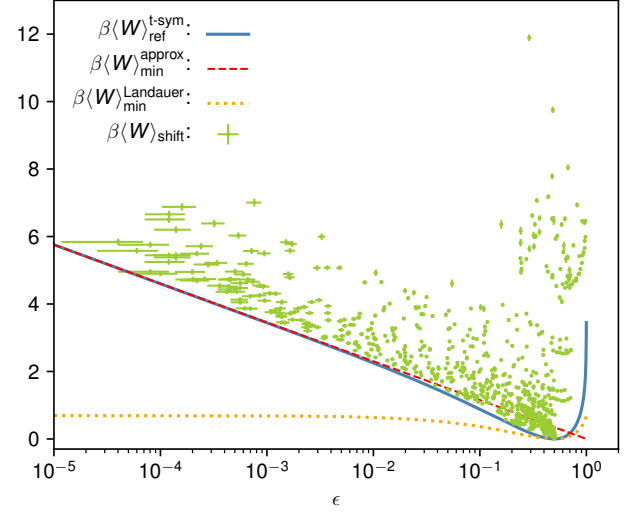


FIG. 10. Reference bound $\langle W \rangle_{\text{ref}}^{t\text{-sym}}$ (blue line) lower bounds all of the shifted works $\langle W \rangle_{\text{shift}}$ (green markers), often quite tightly. The approximate bound $\langle W \rangle_{\min}^{\text{approx}}$ (red dashed line) rapidly converges with decreasing error to $\langle W \rangle_{\text{ref}}^{t\text{-sym}}$. Time-asymmetric protocols can do better, needing only to satisfy Landauer's bound $\langle W \rangle_{\min}^{\text{Landauer}}$ (orange dotted line).

Figure 10 shows the shifted average works for all of the simulated protocols in green with error bars in both sampled ϵ and $\langle W \rangle$. Since we shifted the sampled average works, the vertical distance between the $\langle W \rangle_{\text{shift}}$ and $\langle W \rangle_{\text{ref}}^{t\text{-sym}}$ gives the true difference $\langle W \rangle - \langle W \rangle_{\min}^{t\text{-sym}}$ between the average sampled work and exact bound for the simulated protocol. We see that all simulated protocols satisfy the bound $\langle W \rangle \geq \langle W \rangle_{\min}^{t\text{-sym}}$ and therefore $\langle W_{\text{diss}} \rangle \geq \langle W_{\text{diss}} \rangle_{\min}^{t\text{-sym}}$. Furthermore, many simulated protocols end up quite close to their exact bound. There are protocols with small errors, but they have larger average works. The error-dissipation tradeoff is clear.

Additionally, Fig. 10 shows the low- ϵ asymptotic bound $\langle W \rangle_{\min}^{\text{approx}}$ given by Eqs. (31) and (33). In this semi-log plot, it rather quickly becomes an accurate approximation for small error.

Finally, Fig. 10 plots the Landauer bound $\langle W \rangle_{\min}^{\text{Landauer}}$ as a dotted orange line. It is calculated using ϵ instead of the average error $\langle \epsilon \rangle = 1/2(\epsilon_L + \epsilon_R)$. All shifted average works were either below their true averages or the shifted and true average works were both well above the Landauer bound. And, for most of the simulated protocols, $\epsilon_L \approx \epsilon_R$. So, while the Landauer curve is not a strict bound as presented, it does give an approximate bound for the shifted average works of most simulated protocols. More importantly: as $\epsilon \rightarrow 0$, the relentlessly increasing gap between $\langle W \rangle_{\text{ref}}^{t\text{-sym}}$ and $\langle W \rangle_{\min}^{\text{Landauer}}$, apparent in Fig. 10, highlights the stark difference in energetic scale

between the time-symmetric bounds developed here and the looser Landauer bound. Our time-symmetric bounds are markedly tighter than Landauer's.

Notably, the protocol Landauer originally proposed to erase a bit requires *significantly more work* than his bound $k_B T \ln 2$ to reliably erase a bit. This extra cost is a direct consequence of his protocol's time symmetry. It turns out that time-*asymmetric* protocols for bit erasure have been used in experiments that more nearly approach Landauer's bound [39, 40]. Although, it is not clear to what extent time asymmetry was an intentional design constraint in their construction, since there was no general theoretical guidance until now for why time-symmetry or asymmetry should matter. Figures 10 and 9 confirm that Ref. [40]'s time-asymmetric protocol for bit erasure—where the barrier is lowered before the tilt, but then raised before untilting—is capable of reliable erasure that is more thermodynamically efficient than any time-symmetric protocol could ever be.

B. Logic Gates

We next consider the minimal dissipation required to implement conventional two-input one-output logic gates that serve as the basis for modern digital computing: AND, NAND, OR, NOR, XOR, and the like. The typical implementation requires two bistable memory elements ($\mathcal{M}_t^{(\text{in}_1)}$ and $\mathcal{M}_t^{(\text{in}_2)}$) for the input and another bistable memory element ($\mathcal{M}_t^{(\text{out})}$) to robustly store the output. Each memory element can take on one of two memory states $\mathcal{M}_t^{(\cdot)} \in \{0, 1\}$. Each logic gate is a computation \mathcal{C} on the set of composite memory states $\mathcal{M} = \mathcal{M}^{(\text{in}_1)} \times \mathcal{M}^{(\text{in}_2)} \times \mathcal{M}^{(\text{out})} = \{000, 001, 010, \dots, 111\}$.

In particular, since networks of NAND gates are sufficient for universal computation, the NAND gate is worthy of immediate investigation. Appendix F analyzes the NAND gate, showing that: *if the memory elements are initiated statistically independent of each other*, then the minimal time-symmetric-implementation dissipation is comparable to that expected for bit erasure of the output bit, depending on how often the output bit is overwritten. However, when the memory system is initialized with correlation among the memory elements (perhaps as the correlated output of previous upstream computations), then the change in memory entropy is $\Delta H(\mathcal{M}_t) \approx -H(\mathcal{M}_0^{(\text{out})} | \mathcal{M}_0^{(\text{in}_1)}, \mathcal{M}_0^{(\text{in}_2)})$ in the small ϵ limit, and the reciprocity coefficient is $\langle [\mathcal{C}_{\text{NAND}}(\mathcal{C}_{\text{NAND}}(\mathcal{M}_0)) \neq \mathcal{M}_0] \rangle_{\mathcal{M}_0} = \mu_0(000) + \mu_0(010) + \mu_0(100) + \mu_0(111)$. As a consequence, the initial correlation among the memory elements has a profound impact on the coefficient of minimal dissipation. The overall dissipation still diverges

$\sim \ln(\epsilon^{-1})$, though, with increasing reliability as long as the implementation is time-symmetric.

This example highlights a previously unsuspected source of unnecessary and preventable dissipation in real computers. Indeed, computations are currently implemented in hardware, whether via periodic clocking or static gate voltages, through time-symmetric driving. Error rates in today's reliable digital computers are extremely low. The so-called *soft error rate* (also known as *single-event upsets*) for 50 nm gate technology has been estimated to be on the order of 10^{-4} errors per 10^9 hours of operation of a CMOS logic circuit [41]. Moreover, these errors are overwhelmingly due to cosmic rays rather than conventional thermal fluctuations. If the computer is properly shielded, the error rate is yet significantly lower. Using the aforementioned numbers for a conservative estimate and assuming a 3 GHz clock rate, this extreme reliability of $\epsilon \lesssim 10^{-26}$ errors/instruction would imply at least $30 k_B T$ is dissipated in nearly every elementary operation in modern circuitry directly due to time-symmetric implementation. This is well beyond the Landauer bound that, for NAND and any other traditional two-input-one-output logic gate, is given by $-\Delta H(\mathcal{M}_t) \approx H(\mathcal{M}_0^{(\text{out})} | \mathcal{M}_0^{(\text{in}_1)}, \mathcal{M}_0^{(\text{in}_2)}) \leq \ln 2$.

By way of contrast, the universal Fredkin gate (which swaps the state of its first two memory elements only if the third memory element is in state 1) is not only logically reversible, but is also a strictly-reciprocal gate. As a strictly-reciprocal gate, it can implement universal computation efficiently using time-symmetric control. This makes Fredkin gates an especially tempting basis for energetically-efficient future computing technologies, assuming they can be made to transform metastable memories without the exponential sensitivity to initial conditions that condemned their initially-proposed mechanical instantiation [1, 42].

C. Dissipation in Biological Processing

Beyond logical computation, the reliability-energy-efficiency tradeoff also applies to information processing in far-from-equilibrium biological systems. For this, it is useful to reformulate Eq. (2) to apply when W_{diss} is the work dissipated in controlling (through $x_{0,\tau}$) a system already maintained out of equilibrium by a given housekeeping entropy production Σ_{hk} . This can happen, for example, via ATP hydrolysis or the maintenance of a chemical potential gradient. Then, according to Eq. (27)

of Ref. [43], the more general starting point is:

$$\beta W_{\text{diss}} + k_B^{-1} \Sigma_{\text{hk}} = \ln \left(\frac{\Pr_{x_{0:\tau}}(\mathcal{S}_{0:\tau} = s_{0:\tau} | \mathcal{S}_0 \sim \boldsymbol{\mu}_0)}{\Pr_{\boldsymbol{\mathfrak{A}}(x_{0:\tau})}(\mathcal{S}_{0:\tau} = \boldsymbol{\mathfrak{A}}(s_{0:\tau}) | \mathcal{S}_0 \sim \boldsymbol{\mu}_\tau^\dagger)} \right). \quad (36)$$

In steady-state biological processes, there is no external control. The controllable parameters can thus be considered as held constant, such that the driving protocol is trivially time-symmetric $\boldsymbol{\mathfrak{A}}(x_{0:\tau}) = x_{0:\tau} = x_0 x_1 \dots x_\tau$ and $W_{\text{diss}} = 0$. That is, the system is driven solely by the housekeeping entropy production—power supplied from a stationary stochastic influence—that maintains the steady state. For example, molecular machines can sustain time-asymmetric functionality within their time-symmetric ambient chemical environment⁹ due to the entropy they produce during chemical catalysis [14, 17]. In these nonequilibrium steady states, the expected microstate distribution of the system is the time-invariant steady-state distribution:

$$\boldsymbol{\mu}_0 = \boldsymbol{\mu}_\tau = \boldsymbol{\pi}_{\text{s.s.}} \quad (37)$$

Moreover, due to the low Reynolds numbers of the microbiological realm, momentum is heavily damped and the relevant memory states are time-reversal-invariant: $m^\dagger = m$ for all $m \in \mathcal{M}$. We also have $\boldsymbol{\pi}_{\text{s.s.}}^\dagger = \boldsymbol{\pi}_{\text{s.s.}}$.

Integrating these generic features of steady-state biological transformations, Eq. (36) simplifies to:

$$k_B^{-1} \Sigma_{\text{hk}} = \ln \left(\frac{\Pr(\mathcal{S}_{0:\tau} = s_{0:\tau} | \mathcal{S}_0 = s_0) \boldsymbol{\pi}_{\text{s.s.}}(s_0)}{\Pr(\mathcal{S}_{0:\tau} = \boldsymbol{\mathfrak{A}}(s_{0:\tau}) | \mathcal{S}_0 = s_\tau) \boldsymbol{\pi}_{\text{s.s.}}(s_\tau)} \right). \quad (38)$$

The single-timestep version of Eq. (38) is well known:

$$\delta \Sigma_{\text{hk}} = k_B \ln \left(\frac{\Pr(\mathcal{S}_{\delta t} = s_{\delta t} | \mathcal{S}_0 = s_0) \boldsymbol{\pi}_{\text{s.s.}}(s_0)}{\Pr(\mathcal{S}_{0:\tau} = s_0 | \mathcal{S}_0 = s_{\delta t}) \boldsymbol{\pi}_{\text{s.s.}}(s_{\delta t})} \right).$$

As $\delta t \rightarrow 0$, the relative probabilities reduce to the relative transition rates $\{r_{s \rightarrow s'}\}$:

$$\delta \Sigma_{\text{hk}} = k_B \ln \left(\frac{\boldsymbol{\pi}_{\text{s.s.}}(s_0) r_{s_0 \rightarrow s_{\delta t}}}{\boldsymbol{\pi}_{\text{s.s.}}(s_{\delta t}) r_{s_{\delta t} \rightarrow s_0}} \right). \quad (39)$$

(Metastability of mesoscopic conformations allows Eq. (39) to hold approximately for transitions between mesoscopic states as well.) For example, Eq. (39) was the starting point for the recently-derived thermodynamic uncertainty relations [44] which have received considerable attention.

However, much can be learned from approaching finite-duration transformations directly, by coarse-graining Eq. (38) according to initial and final functionally-relevant states. Notably, it allows simple yet powerful analysis of the minimal dissipation required for biological functionality, regardless of how complicated the finite-duration biological implementations appear. And, it implies a generic error–dissipation tradeoff that we expect to apply broadly to the reliable performance of microbiological systems.

Working this out explicitly leads to a pleasantly simple picture of steady-state biological information processing and its requisite dissipation:

$$\begin{aligned} k_B^{-1} \langle \Sigma_{\text{hk}} \rangle &\geq D_{\text{KL}} [\Pr(\mathcal{M}_0 = m, \mathcal{M}_\tau = m') \parallel \Pr(\mathcal{M}_\tau = m', \mathcal{M}_{2\tau} = m)] \\ &= \underbrace{\Delta H(\mathcal{M}_t)}_{=0 \text{ since } \boldsymbol{\mu}_\tau = \boldsymbol{\mu}_0 = \boldsymbol{\pi}_{\text{s.s.}}} + \sum_{m, m' \in \mathcal{M}} \boldsymbol{\pi}_{\text{s.s.}}(m) p(m \rightarrow m') \ln \frac{p(m \rightarrow m')}{p(m' \rightarrow m)} \\ &= \sum_{m, m' \in \mathcal{M}} \boldsymbol{\pi}_{\text{s.s.}}(m) p(m \rightarrow m') \Psi(m \rightarrow m') \\ &= \langle \Psi(\mathcal{M} \rightarrow \mathcal{M}') \rangle_{\boldsymbol{\pi}_{\text{s.s.}}(\mathcal{M}) p(\mathcal{M} \rightarrow \mathcal{M}')} \end{aligned} \quad (40)$$

Steady-state computation quite simply becomes the en-

forcement of a Markov model for memory transitions $\{p(m \rightarrow m')\}$. The minimal dissipation achievable via any biological implementation is equal to the expected nonreciprocity. It should be noted that the steady state distribution over memory states $\boldsymbol{\pi}_{\text{s.s.}}$ is easily found as

⁹ This time-symmetric ambient chemical environment is maintained by power-consuming homeostatic mechanisms elsewhere in a cell.

the stationary eigenstate of the Markov model's transition matrix.

In equilibrium, where $\pi_{\text{s.s.}} = \pi_{\text{eq}}$, the average nonreciprocity vanishes since then detailed balance demands $\pi_{\text{eq}}(m)p_{\text{eq}}(m \rightarrow m') = \pi_{\text{eq}}(m')p_{\text{eq}}(m' \rightarrow m)$ while, as always, $\Psi(m \rightarrow m') = -\Psi(m' \rightarrow m)$. As necessary, this allows zero dissipation in equilibrium. In contrast, nonequilibrium steady-state computations must dissipate because they bias nonreciprocated transitions. These computations enforce nondetailed-balanced dynamics.

Equation (40) shows that dissipation in steady-state biological processes is bounded by the average nonreciprocity. Remarkably, this bound depends only on the net transformation and is independent of any intermediary steps or biochemical details that could be involved.

Thus, as in the preceding analysis, one expects a generic error–dissipation tradeoff:

$$d\Sigma_{\text{hk}}/dt \propto \ln(1/\epsilon)$$

for reliable steady-state biological transformations of genetic information—whenever certain transitions need to be strongly enforced with only a small probability of failure ϵ . The generic error–dissipation tradeoff holds, as an important example, for processes such as chemical proof-reading necessary for reliable DNA replication. In this way, our contribution dovetails with more model-specific results on the latter by Refs. [45–48]. Since codons are nonreciprocally corrected to satisfy Watson–Crick base pairing, each correction will require significant dissipation.

The $d\Sigma_{\text{hk}}/dt \propto \ln(1/\epsilon)$ error–dissipation tradeoff should arise in other reliable biological transformations as well. For example, Ref. [49] finds exactly this minimum dissipation rate is needed to reliably maintain a target nonequilibrium state. This is relevant to protein folding, as well as other biological functionalities.

Our results also support and update the perspective of Ref. [50], where steady-state biochemical copying networks (e.g., for sensing) were found to have an unavoidable error–dissipation tradeoff due to the time-invariant driving. Our results more broadly suggest an error–dissipation tradeoff for any biochemical task with nonreciprocity. It should now be clear that autonomous biochemical systems in steady state can never reach the Landauer bound on efficiency because of the time-symmetric control penalty.

V. CONCLUSION

We found that time symmetry and metastability together imply a generic error–dissipation tradeoff. The minimal

work expected for a computation \mathcal{C} is the average nonreciprocity. In the low-error limit—where the probability of error must be less than ϵ —the minimum work diverges according to:

$$\beta\langle W \rangle_{\min}^{\text{approx}} = \langle [\mathcal{C}(\mathcal{M}_0)^\dagger]^\dagger \neq \mathcal{M}_0 \rangle_{\mathcal{M}_0} \ln(\epsilon^{-1})$$

Of all of this work, only the meager Landauer cost $\Delta H(\mathcal{M}_t)$, which saturates to some finite value as $\epsilon \rightarrow 0$, can be recovered in principle. Thus, irretrievable dissipation scales as $\ln(\epsilon^{-1})$. The reciprocity coefficient $\langle [\mathcal{C}(\mathcal{M}_0)^\dagger]^\dagger \neq \mathcal{M}_0 \rangle_{\mathcal{M}_0}$ depends only on the deterministic computation to be approximated. This points out likely energetic inefficiencies in current instantiations of reliable computation. It also suggests that time-asymmetric control may allow more efficient computation—but only when time-asymmetry is a free resource.

Restricting to time-symmetric driving may seem unusual. However, with the time-symmetric clock signal that drives modern microprocessors, it is the norm rather than the exception in the realm of informational controls. Sections IV B and IV C discussed the naturalness of time-symmetry in digital computers and in genetic processing, respectively. To get there, though, required developing several prerequisite thermodynamic results.

After developing the general thermodynamics, we analyzed the limit of highly-reliable computing. As important examples, we then specialized to dissipation in erasure, logic gates, and reliable biological transformations.

We now close with brief comments on related results and future directions.

A. Related Results

It is worth considering how our results—that revealed the tradeoff between accuracy and energetic-efficiency under time-symmetric protocols—compare to related approaches to thermodynamic control, both historically and today.

In Ref. [51], Brillouin defines the reliability as $1/\epsilon$, where ϵ is the probability of reading out the wrong value due to thermal agitation. He found that the entropy production necessary for some methods of reliable *readout* is $k_B \ln(1/\epsilon)$. It is interesting that Brillouin's readout result mirrors the same error–dissipation scaling as found in our analysis, despite the fact that detailed fluctuation theorems, the foundations of our analysis, were still decades away. Brillouin's readout penalty is distinct from our result, but it hints at a more general error–dissipation tradeoff (under particular physical constraints) that could unite the results.

Brillouin's readout penalty also appeared in disguise in Ref. [52], which again, superficially, appears to propose a

similar error–dissipation tradeoff to what we have identified. As in Ref. [53], Ref. [52] defines a ‘logic operation’ specifically as bit inversion, $0 \mapsto 1$ and $1 \mapsto 0$ —a strictly reciprocal computation. Reference [52] thus defines the “minimal work per logic operation” as the minimal work for bit inversion. Despite similarities in appearance, it is clearly different from our result since it predicts divergent dissipation for reliable implementation of a strictly-reciprocal computation. In this setting, if the voltage drifts from one input to the other (a readout error), then the wrong input will be inverted. While some computational implementations may require further inefficiency to avoid this source of error, it is distinct and perhaps additive to our nonreciprocity dissipation.

A discussion of reliable computing would be incomplete without mention of error-correction [54]. Indeed, it might seem plausible that less reliable components could be used to avoid the error–dissipation tradeoff while nevertheless achieving the same net reliability through error correction. However, we have found that error correction via redundancy only leads to a *worse* error–dissipation tradeoff when the dissipation from all components is considered. We will report on this elsewhere.

More recently, there are complementary results suggesting that various restrictions on control lead to additional work beyond the Landauer bound and so to dissipation. For instance, if constrained to operate in finite time τ , the dissipation using *optimal* protocols scales as the inverse τ^{-1} of the protocol’s duration. The three-way tradeoff between accuracy, speed, and energy efficiency has been explored recently in several settings [11, 47, 55–57]. These suggest that if performed sufficiently slowly, an information processing protocol could achieve the Landauer bound, with zero excess dissipation. In contrast, we found that for time-symmetric protocols, the dissipation scales as $\ln(\epsilon^{-1})$. Thus, one cannot achieve the Landauer bound, no matter how slowly the protocol is executed. In this, our result is more akin to other recently explored control restrictions, such as modularity [5, 33]. This too prevents efficient extraction of nonequilibrium free energy, no matter how slowly the protocol is executed.

Our results highlight using time-asymmetric control for more energetically efficient computation, but is time-asymmetry ever free? Often in the thermodynamics of control, one assumes that there is an external signal that can be produced in any sequence, reversible or not, at no cost beyond the work-energy imparted to the driven system. Inexpensive time asymmetry can be generated, for example, from inertial degrees of freedom [38].

However, in biological systems and in many engineered nanoscale systems, inertial degrees of freedom are not available. Noninertial batteries reliably transforming

noninertial systems will drain according to our time-symmetric-control bounds on dissipation.

Time-symmetric control might also seem to apply, rather broadly, if one removes the boundaries separating a driven system from its driver. Including the driver as part of an enlarged system gives the appearance of trivially time-symmetric driving of the composite system. Do our time-symmetric-control bounds on dissipation then apply to any reliable computations that occur within this enlarged system? Generically, our bounds will *not* apply to such enlarged systems because the enlarged microstate distributions μ_0 and μ_τ will no longer be metastable.

This suggests that time-asymmetry and instability can both lead to energetic advantages. In future work, we explore *which* features of time-asymmetry matter for efficiency. This will help identify those qualitative features of time-symmetric control that need to be overcome for greater efficiency.

For time-symmetric protocols, we now ask: How does ϵ scale with τ or with the modularity of control? Generically, we do not expect a one-to-one relationship between the error and duration. Rather, generally, there will be a high-dimensional space of tradeoff scalings that includes speed, error, modularity of control, robustness of information storage, energetic efficiency, and many other computationally relevant design restrictions.

B. Looking Forward

The results derived here elevate time-asymmetric control to a *design principle* for efficient thermodynamic computing. This then must be added to the growing list of recently-discovered principles, including tracking system modularity [5, 33] and logic gates whose protocols adapt to their input [5]. Progress will turn on how these lessons are incorporated as constraints in the principled design and search for near-optimal finite-time protocols. An opportunity presents itself to adapt these lessons to developing fast hyper-efficient computers in the not-so-distant future.

ACKNOWLEDGMENTS

The authors thank Gavin Crooks, Mike DeWeese, and Chris Jarzynski for helpful discussions and the Telluride Science Research Center for hospitality during visits and the participants of the Information Engines Workshops there. JPC acknowledges the kind hospitality of the Santa Fe Institute, Institute for Advanced Study at the University of Amsterdam, and California Institute of Technology

for their hospitality during visits. This material is based upon work supported by, or in part by, FQXi Grant number FQXi-RFP-1609, the John Templeton Foundation grant 52095, Templeton World Charity Foundation Power of Information fellowship TWCF0337, and U. S. Army Research Laboratory and the U. S. Army Research Office under contracts W911NF-13-1-0390 and W911NF-18-1-0028.

Appendix A: Dissipated-work bounds

1. General observation channels

Given a probability distribution over microstate trajectories for forward driving $\rho(\mathcal{S}_{0:\tau} = s_{0:\tau}) = \Pr_{x_{0:\tau}}(\mathcal{S}_{0:\tau} = s_{0:\tau} | \mathcal{S}_0 \sim \boldsymbol{\mu}_0)$ and reverse driving $\rho^R(\mathcal{S}_{0:\tau} = s_{0:\tau}) = \Pr_{\mathbf{J}(x_{0:\tau})}(\mathcal{S}_{0:\tau} = \mathbf{J}(s_{0:\tau}) | \mathcal{S}_0 \sim \boldsymbol{\mu}_\tau^\dagger)$, the dissipated work is proportional to the relative entropy:

$$\beta \langle W_{\text{diss}} \rangle = D_{\text{KL}} [\rho(\mathcal{S}_{0:\tau}) \parallel \rho^R(\mathcal{S}_{0:\tau})] . \quad (\text{A1})$$

However, in practice, observing microstate trajectories is impractical. Any observational instrument will only give partial information about the microstate trajectory and only provide a probability over an observational variable \vec{Y} under reverse or forward driving. Generally, such an observational device can be characterized as a noisy channel Γ that probabilistically maps joint microstate trajectories $(s_{0:\tau}, x_{0:\tau})$ to observations \vec{y} :

$$\Gamma_{s_{0:\tau}, x_{0:\tau} \rightarrow \vec{y}} = \Pr(\vec{Y} = \vec{y} | \mathcal{S}_{0:\tau} = s_{0:\tau}, \mathcal{X}_{0:\tau} = x_{0:\tau}) . \quad (\text{A2})$$

In many cases—as with the coarse-grainings of system trajectories $s_{0:\tau}$ primarily considered in the main text—the observation channel has no dependence on the driving:

$$\begin{aligned} \Gamma_{s_{0:\tau}, x_{0:\tau} \rightarrow \vec{y}} &= \Gamma_{s_{0:\tau} \rightarrow \vec{y}} \\ &= \Pr(\vec{Y} = \vec{y} | \mathcal{S}_{0:\tau} = s_{0:\tau}) . \end{aligned} \quad (\text{A3})$$

Notably, the observation channel then has no dependence on the driving $x_{0:\tau}$, although the driving would still influence the actualized microstate trajectory which is *input* to the channel.

We use the more general Eq. (A2) to define joint proba-

bilities over observations and microstate trajectories:¹⁰

$$\begin{aligned} \rho(\vec{Y} = \vec{y}, \mathcal{S}_{0:\tau} = s_{0:\tau}) &= \Pr_{x_{0:\tau}}(\vec{Y} = \vec{y}, \mathcal{S}_{0:\tau} = s_{0:\tau} | \mathcal{S}_0 \sim \boldsymbol{\mu}_0) \\ &= \Gamma_{s_{0:\tau}, x_{0:\tau} \rightarrow \vec{y}} \rho(\mathcal{S}_{0:\tau} = s_{0:\tau}) . \end{aligned}$$

We also define the reverse joint probability as the probability of obtaining the reverse observation and reverse microstate trajectory under the reverse protocol:

$$\begin{aligned} \rho^R(\vec{Y} = \vec{y}, \mathcal{S}_{0:\tau} = s_{0:\tau}) &= \Pr_{\mathbf{J}(x_{0:\tau})}(\vec{Y} = \mathbf{J}(\vec{y}), \mathcal{S}_{0:\tau} = \mathbf{J}(s_{0:\tau}) | \mathcal{S}_0 \sim \boldsymbol{\mu}_\tau^\dagger) \\ &= \Gamma_{\mathbf{J}(s_{0:\tau}), \mathbf{J}(x_{0:\tau}) \rightarrow \mathbf{J}(\vec{y})} \rho^R(\mathcal{S}_{0:\tau} = s_{0:\tau}) , \end{aligned}$$

where the time reversal $\mathbf{J}(\vec{y})$ of the observed variable \vec{y} must be defined by the observer.

The definition of $\mathbf{J}(\vec{y})$ is most *useful* in bounding dissipation when it corresponds to a true time-reversal of some sequence of physical observables. For example, if the observable is a deterministic function of the joint microstate dynamics $\vec{y} = f(s_{0:\tau}, x_{0:\tau})$, then it might be the case that:

$$\mathbf{J}(\vec{y}) = f(\mathbf{J}(s_{0:\tau}), \mathbf{J}(x_{0:\tau})) . \quad (\text{A4})$$

This is true when the observable is work $w = \int_0^\tau \frac{\partial E_{x_t}(s_t)}{\partial x_t} dx_t$. Work and its reversal—observed, e.g., via how high a weight has been raised—are related by: $\mathbf{J}(w(s_{0:\tau}, x_{0:\tau})) = w(\mathbf{J}(s_{0:\tau}), \mathbf{J}(x_{0:\tau})) = -w(s_{0:\tau}, x_{0:\tau})$. Equation (A4) is also true when the observable is a coarse graining of the microstate trajectory as utilized for our main results: $f(s_{0:\tau}, x_{0:\tau}) = (s_0, s_\tau) \implies \mathbf{J}(f(s_{0:\tau}, x_{0:\tau})) = f(\mathbf{J}(s_{0:\tau}), \mathbf{J}(x_{0:\tau})) = (s_\tau^\dagger, s_0^\dagger)$. Noisy channels can also satisfy a stochastic version of Eq. (A4).

Fortunately, in some cases, information derived from the sort of general observational channel described in Eq. (A2) allows us to put a bound on the dissipated work using the chain rule of relative entropy [24]. The chain rule states that the relative entropy of the two distributions p and q over two variables X and Y can be broken into the sum of nonnegative terms:

$$\begin{aligned} D_{\text{KL}} [p(X, Y) \parallel q(X, Y)] \\ = D_{\text{KL}} [p(X) \parallel q(X)] + D_{\text{KL}} [p(Y|X) \parallel q(Y|X)] , \end{aligned}$$

¹⁰ The more general Eq. (A2) is necessary, for example, to include mechanical work as an observable, since mechanical work is a functional of both the driving $x_{0:\tau}$ and the system's microstate trajectory $s_{0:\tau}$.

where:

$$\begin{aligned} & D_{\text{KL}} [p(Y|X) \parallel q(Y|X)] \\ &= \sum_x p(X=x) \sum_y p(Y=y|X=x) \ln \frac{p(Y=y|X=x)}{q(Y=y|X=x)}, \end{aligned}$$

is zero if and only if $p(Y=y|X=x) = q(Y=y|X=x)$ for all x and y . Applying this result to obtain two different decompositions of $D_{\text{KL}} [\rho(\vec{Y}, \mathcal{S}_{0:\tau}) \parallel \rho^R(\vec{Y}, \mathcal{S}_{0:\tau})]$, relating the observed variables and microstate trajectories, we see:

$$D_{\text{KL}} [\rho(\mathcal{S}_{0:\tau}) \parallel \rho^R(\mathcal{S}_{0:\tau})] = D_{\text{KL}} [\rho(\vec{Y}) \parallel \rho^R(\vec{Y})] + D_{\text{KL}} [\rho(\mathcal{S}_{0:\tau}|\vec{Y}) \parallel \rho^R(\mathcal{S}_{0:\tau}|\vec{Y})] - D_{\text{KL}} [\rho(\vec{Y}|\mathcal{S}_{0:\tau}) \parallel \rho^R(\vec{Y}|\mathcal{S}_{0:\tau})]. \quad (\text{A5})$$

We expand the first term on the RHS:

$$D_{\text{KL}} [\rho(\vec{Y}) \parallel \rho^R(\vec{Y})] = D_{\text{KL}} \left[\Pr_{x_{0:\tau}}(\vec{Y} = \vec{y} | \mathcal{S}_0 \sim \mu_0) \parallel \Pr_{\mathbf{J}(x_{0:\tau})}(\vec{Y} = \mathbf{J}(\vec{y}) | \mathcal{S}_0 \sim \mu_\tau^\dagger) \right],$$

where the probability distributions input to the relative entropy are implied by the explicitly-written *elements* of the distribution. The final term can also be rewritten:

$$\begin{aligned} D_{\text{KL}} [\rho(\vec{Y}|\mathcal{S}_{0:\tau}) \parallel \rho^R(\vec{Y}|\mathcal{S}_{0:\tau})] &= \left\langle D_{\text{KL}} \left[\Gamma_{s_{0:\tau}, x_{0:\tau} \rightarrow \vec{Y}} \parallel \Gamma_{\mathbf{J}(s_{0:\tau}), \mathbf{J}(x_{0:\tau}) \rightarrow \mathbf{J}(\vec{Y})} \right] \right\rangle_{\rho(\mathcal{S}_{0:\tau})} \\ &= \frac{1}{k_B} \Sigma_{\text{ch}}, \end{aligned}$$

which (besides a factor of k_B) we call the exhibited *channel irreversibility* Σ_{ch} . Essentially, irreversible observation channels may consume energy and produce their own entropy which could lead to observed irreversibility beyond what is actually produced by the microstate dynamics. (Whereas, unpowered observation channels should be reversible.) However, the definition used for $\mathbf{J}(\vec{y})$ also plays an important role: The channel could appear irreversible simply because one does not utilize the *physical* time reversal of \vec{y} .

Since $D_{\text{KL}} [\rho(\mathcal{S}_{0:\tau}|\vec{Y}) \parallel \rho^R(\mathcal{S}_{0:\tau}|\vec{Y})] \geq 0$, we can now deduce from Eq. (A5) the following bound on the dissipated

work:

$$\beta \langle W_{\text{diss}} \rangle \geq D_{\text{KL}} [\rho(\vec{Y}) \parallel \rho^R(\vec{Y})] - \frac{1}{k_B} \Sigma_{\text{ch}}.$$

This is a promising relationship, since it suggests that we can bound the work production with partial information about microstates. Moreover, channel irreversibility can be reduced or removed by using passive channels and a physically-motivated time-reversal mapping of observables. Specifically, if the mapping from microstate trajectories to observables is preserved under reversal of both trajectories and observations $\Gamma_{\mathbf{J}(s_{0:\tau}), \mathbf{J}(x_{0:\tau}) \rightarrow \mathbf{J}(\vec{Y})} = \Gamma_{s_{0:\tau}, x_{0:\tau} \rightarrow \vec{Y}}$ for all $s_{0:\tau}$ and $x_{0:\tau}$, then the channel irreversibility vanishes. In this case, the dissipated work is bounded by the relative entropy between forward and reverse driving of observables:

$$\beta \langle W_{\text{diss}} \rangle \geq D_{\text{KL}} \left[\Pr_{x_{0:\tau}}(\vec{Y} = \vec{y} | \mathcal{S}_0 \sim \mu_0) \parallel \Pr_{\mathbf{J}(x_{0:\tau})}(\vec{Y} = \mathbf{J}(\vec{y}) | \mathcal{S}_0 \sim \mu_\tau^\dagger) \right], \quad (\text{A6})$$

where, again and in the following, the probability dis-

tributions for the relative entropy are implied by the

explicitly-written elements. This relation gives us a useful tool for bounding the dissipated work given limited information about the microstate dynamics, much as is explored in Refs. [27, 30, 31].

2. Computational coarse-grainings

Not all observational channels Γ satisfy the bound given by Eq. (A6). However, observation channels that coarse-grain the possible microstate trajectories *always* satisfy this bound when the reversal of the coarse-graining $\mathbf{J}(\tilde{y})$ is also an observable element of the coarse graining.

In the following, we consider the case where we observe memory states \mathcal{M} , which are coarse-grainings of the microstates, at the initial and final times. The random variable \mathcal{M}_t for the memory state at time t is completely determined by the random variable for the microstate \mathcal{S}_t . We will also employ an even coarser graining of microstate trajectories that takes microstate trajectories to the pair of starting and ending memory states.

In particular, consider the observational channel (of the simple form of Eq. (A3)) to be a coarse-graining:

$$\Gamma_{s_{0:\tau} \rightarrow mm'} = \delta_{s_0 \in m} \delta_{s_\tau \in m'} ,$$

which leads to the marginal distributions:

$$\rho(\mathcal{M}_0 = m, \mathcal{M}_\tau = m') = \sum_{s_{0:\tau}} \delta_{s_0 \in m} \delta_{s_\tau \in m'} \rho(\mathcal{S}_{0:\tau} = s_{0:\tau})$$

and:

$$\rho^R(\mathcal{M}_0 = m, \mathcal{M}_\tau = m') = \sum_{s_{0:\tau}} \delta_{s_0 \in m} \delta_{s_\tau \in m'} \rho^R(\mathcal{S}_{0:\tau} = s_{0:\tau}) .$$

If we define the reversal of our observations:

$$\mathbf{J}(mm') = (m'^\dagger m^\dagger),$$

where:

$$m^\dagger \equiv \{s^\dagger : s \in m\} ,$$

is also an element of the memory states $m^\dagger \in \mathcal{M}$, then the observational channel is preserved under reversal

$$\begin{aligned} \Gamma_{\mathbf{J}(s_{0:\tau}) \rightarrow \mathbf{J}(mm')} &= \Gamma_{s_\tau^\dagger \dots s_0^\dagger \rightarrow m'^\dagger m^\dagger} \\ &= \delta_{s_\tau^\dagger \in m'^\dagger} \delta_{s_0^\dagger \in m^\dagger} \\ &= \delta_{s_\tau \in m'} \delta_{s_0 \in m} \\ &= \Gamma_{s_{0:\tau} \rightarrow mm'} , \end{aligned}$$

where we've used the fact that $s^\dagger \in m^\dagger \iff s \in m$. Thus, we find for such a partitioning into memory states that the dissipated work is bounded by the relative entropy of the memory state distributions:

$$\beta \langle W_{\text{diss}} \rangle \geq \text{D}_{\text{KL}} \left[\Pr_{x_{0:\tau}} (\mathcal{M}_0 = m, \mathcal{M}_\tau = m' | \mathcal{S}_0 \sim \mu_0) \right] \left\| \Pr_{\mathbf{J}(x_{0:\tau})} (\mathcal{M}_0 = m'^\dagger, \mathcal{M}_\tau = m^\dagger | \mathcal{S}_0 \sim \mu_\tau^\dagger) \right] . \quad (\text{A7})$$

Note that there are partitions for which this does not hold since m^\dagger is not an element of the partition. If there are elements of a particular memory state $s, s' \in m$ such that $s^\dagger \in m'$ but $s'^\dagger \in m'' \neq m'$, then $m^\dagger \notin \mathcal{M}$, meaning that m^\dagger is not itself a memory state. In such a case, it makes no sense to say whether $\mathcal{M}_t = m^\dagger$, since \mathcal{M}_t is the random variable for the memory state and m^\dagger is not a memory state. In these cases, the proof of the bound given in this section is not applicable. The more general scenario is nevertheless addressed by the more general bound Eq. (B1) in App. B.

Appendix B: Dissipated-work bound for computation

For our main results, we consider the case where we observe memory states \mathcal{M} , where \mathcal{M} is a partitioning of the microstates \mathcal{S} , at the initial and final times. The random variable \mathcal{M}_t for the memory state at time t is completely determined by the random variable for the microstate \mathcal{S}_t via the memory coarse-graining function $f_{\mathcal{M}}: \mathcal{S} \rightarrow \mathcal{M}$. In the following, we also utilize an even coarser graining of microstate trajectories which takes microstate trajectories to the pair of starting and ending memory states: $f_{\mathcal{M}_0, \mathcal{M}_\tau}(s_{0:\tau}) = (f_{\mathcal{M}}(s_0), f_{\mathcal{M}}(s_\tau))$.

We begin by deriving a bound on dissipation in terms of

a general partitioning \mathcal{M} .

Note that the two probability distributions $\rho(s_{0:\tau}) \equiv \Pr_{x_{0:\tau}}(\mathcal{S}_{0:\tau} = s_{0:\tau} | \mathcal{S}_0 \sim \mu_0)$ and $\rho^R(s_{0:\tau}) \equiv \Pr_{\mathfrak{A}(x_{0:\tau})}(\mathcal{S}_{0:\tau} = \mathfrak{A}(s_{0:\tau}) | \mathcal{S}_0 \sim \mu_\tau^\dagger)$ each have the same support $s_{0:\tau} \in \mathcal{S}^{[0,\tau]}$. From Eq. (2), the expected dissipated work is: $\langle W_{\text{diss}} \rangle = k_B T D_{\text{KL}}[\rho \parallel \rho^R]$.

Now consider the coarse-grained marginal distributions: $\mathbf{P}(m, m') = \sum_{s_{0:\tau}} \delta_{s_0 \in m} \delta_{s_\tau \in m'} \rho(s_{0:\tau})$ and $\mathbf{Q}(m, m') = \sum_{s_{0:\tau}} \delta_{s_0 \in m} \delta_{s_\tau \in m'} \rho^R(s_{0:\tau})$.

Since the same coarse graining kernel from $\mathcal{S}^{[0,\tau]}$ to \mathcal{M}^2 is applied to each of the distributions ρ and ρ^R , the data-processing inequality for D_{KL} [24] guarantees that: $D_{\text{KL}}[\mathbf{P} \parallel \mathbf{Q}] \leq D_{\text{KL}}[\rho \parallel \rho^R]$.

Moreover, note that:

$$\begin{aligned} \mathbf{P}(m, m') &= \sum_{s_{0:\tau}} \delta_{s_0 \in m} \delta_{s_\tau \in m'} \Pr_{x_{0:\tau}}(\mathcal{S}_{0:\tau} = s_{0:\tau} | \mathcal{S}_0 \sim \mu_0) \\ &= \Pr_{x_{0:\tau}}(\mathcal{M}_0 = m, \mathcal{M}_\tau = m' | \mathcal{S}_0 \sim \mu_0), \end{aligned}$$

and:

$$\begin{aligned} \mathbf{Q}(m, m') &= \sum_{s_{0:\tau}} \delta_{s_0 \in m} \delta_{s_\tau \in m'} \Pr_{\mathfrak{A}(x_{0:\tau})}(\mathcal{S}_{0:\tau} = \mathfrak{A}(s_{0:\tau}) | \mathcal{S}_0 \sim \mu_\tau^\dagger) \\ &= \Pr_{\mathfrak{A}(x_{0:\tau})}(\mathcal{S}_0 \in m'^\dagger, \mathcal{S}_\tau \in m^\dagger | \mathcal{S}_0 \sim \mu_\tau^\dagger). \end{aligned}$$

Hence, we have shown that the dissipated work is always lower-bounded by a function of the net transition probabilities between memory states:

$$\begin{aligned} \beta \langle W_{\text{diss}} \rangle &= D_{\text{KL}} \left[\Pr_{x_{0:\tau}}(\mathcal{S}_{0:\tau} = s_{0:\tau} | \mathcal{S}_0 \sim \mu_0) \parallel \Pr_{\mathfrak{A}(x_{0:\tau})}(\mathcal{S}_{0:\tau} = \mathfrak{A}(s_{0:\tau}) | \mathcal{S}_0 \sim \mu_\tau^\dagger) \right] \\ &\geq D_{\text{KL}} \left[\Pr_{x_{0:\tau}}(\mathcal{M}_0 = m, \mathcal{M}_\tau = m' | \mathcal{S}_0 \sim \mu_0) \parallel \Pr_{\mathfrak{A}(x_{0:\tau})}(\mathcal{S}_0 \in m'^\dagger, \mathcal{S}_\tau \in m^\dagger | \mathcal{S}_0 \sim \mu_\tau^\dagger) \right]. \end{aligned} \quad (\text{B1})$$

Equation (B1) is valid even when $m^\dagger \notin \mathcal{M}$.

When $m^\dagger \in \mathcal{M}$ for all $m \in \mathcal{M}$, Eq. (B1) clearly reduces to:

$$\beta \langle W_{\text{diss}} \rangle \geq D_{\text{KL}} \left[\Pr_{x_{0:\tau}}(\mathcal{M}_0 = m, \mathcal{M}_\tau = m' | \mathcal{S}_0 \sim \mu_0) \parallel \Pr_{\mathfrak{A}(x_{0:\tau})}(\mathcal{M}_0 = m'^\dagger, \mathcal{M}_\tau = m^\dagger | \mathcal{S}_0 \sim \mu_\tau^\dagger) \right], \quad (\text{B2})$$

in agreement with the alternative derivation that led to Eq. (A7). Equation (B2) will be broadly applicable to computations performed on positional, configurational, or typical magnetic memory systems. Indeed, there are many standard types of memory states which satisfy $m^\dagger \in \mathcal{M}$, so that Eq. (B2) is applicable. For example, positionally partitioned states are often used to store information in systems with potential energy minima at different spatial locations. (As implemented in, for example, Maxwell demon experiments via laser ion traps, also called ‘optical tweezers’ when the location of these traps is dynamically controlled.) These positional memories have a clear defini-

tion of time reversal in which $m^\dagger = m$. This follows since if $s = (\vec{q}, \vec{\varphi})$ is in m , then so is $s^\dagger = (\vec{q}, -\vec{\varphi})$. Another form of memory state utilizes magnetic spins, for which the time reversal flips all microstate spins—spin-up maps to spin-down upon time-reversal, and vice versa. In the case of bistable magnetic memory elements, the time-reversal of any memory is also a valid memory $m^\dagger \in \mathcal{M}$, although $m^\dagger \neq m$. Thus, for both of these forms of memory, the reversal of a memory state is an element of the partitioning, so that Eq. (B2) is applicable.

Further decomposing Eq. (B2), we find:

$$\begin{aligned}
\beta \langle W_{\text{diss}} \rangle &\geq \text{D}_{\text{KL}} \left[\Pr_{x_{0:\tau}}(\mathcal{M}_0 = m, \mathcal{M}_\tau = m' | \mathcal{S}_0 \sim \boldsymbol{\mu}_0) \parallel \Pr_{\mathbf{J}(x_{0:\tau})}(\mathcal{M}_0 = m^\dagger, \mathcal{M}_\tau = m^\dagger | \mathcal{S}_0 \sim \boldsymbol{\mu}_\tau^\dagger) \right] \\
&= \sum_{m, m' \in \mathcal{M}} \Pr_{x_{0:\tau}}(\mathcal{M}_0 = m, \mathcal{M}_\tau = m' | \mathcal{S}_0 \sim \boldsymbol{\mu}_0) \ln \left(\frac{\Pr_{x_{0:\tau}}(\mathcal{M}_0 = m, \mathcal{M}_\tau = m' | \mathcal{S}_0 \sim \boldsymbol{\mu}_0)}{\Pr_{\mathbf{J}(x_{0:\tau})}(\mathcal{M}_0 = m^\dagger, \mathcal{M}_\tau = m^\dagger | \mathcal{S}_0 \sim \boldsymbol{\mu}_\tau^\dagger)} \right) \\
&= \sum_{m, m' \in \mathcal{M}} \Pr_{x_{0:\tau}}(\mathcal{M}_0 = m, \mathcal{M}_\tau = m' | \mathcal{S}_0 \sim \boldsymbol{\mu}_0) \\
&\quad \times \ln \left(\frac{\Pr_{x_{0:\tau}}(\mathcal{M}_0 = m | \mathcal{S}_0 \sim \boldsymbol{\mu}_0) \Pr_{x_{0:\tau}}(\mathcal{M}_\tau = m' | \mathcal{S}_0 \sim \boldsymbol{\mu}_0, \mathcal{M}_0 = m)}{\Pr_{\mathbf{J}(x_{0:\tau})}(\mathcal{M}_0 = m^\dagger | \mathcal{S}_0 \sim \boldsymbol{\mu}_\tau^\dagger) \Pr_{\mathbf{J}(x_{0:\tau})}(\mathcal{M}_\tau = m^\dagger | \mathcal{S}_0 \sim \boldsymbol{\mu}_\tau^\dagger, \mathcal{M}_0 = m^\dagger)} \right) \\
&= \sum_{m, m' \in \mathcal{M}} \Pr_{x_{0:\tau}}(\mathcal{M}_0 = m, \mathcal{M}_\tau = m' | \mathcal{S}_0 \sim \boldsymbol{\mu}_0) \ln \left(\Pr_{x_{0:\tau}}(\mathcal{M}_0 = m | \mathcal{S}_0 \sim \boldsymbol{\mu}_0) \right) \\
&\quad - \sum_{m, m' \in \mathcal{M}} \Pr_{x_{0:\tau}}(\mathcal{M}_0 = m, \mathcal{M}_\tau = m' | \mathcal{S}_0 \sim \boldsymbol{\mu}_0) \ln \left(\Pr_{\mathbf{J}(x_{0:\tau})}(\mathcal{M}_0 = m^\dagger | \mathcal{S}_0 \sim \boldsymbol{\mu}_\tau^\dagger) \right) \\
&\quad + \sum_{m, m' \in \mathcal{M}} \Pr_{x_{0:\tau}}(\mathcal{M}_0 = m, \mathcal{M}_\tau = m' | \mathcal{S}_0 \sim \boldsymbol{\mu}_0) \ln \left(\frac{\Pr_{x_{0:\tau}}(\mathcal{M}_\tau = m' | \mathcal{S}_0 \sim \boldsymbol{\mu}_0, \mathcal{M}_0 = m)}{\Pr_{\mathbf{J}(x_{0:\tau})}(\mathcal{M}_\tau = m^\dagger | \mathcal{S}_0 \sim \boldsymbol{\mu}_\tau^\dagger, \mathcal{M}_0 = m^\dagger)} \right) \\
&= \sum_{m \in \mathcal{M}} \Pr_{x_{0:\tau}}(\mathcal{M}_0 = m | \mathcal{S}_0 \sim \boldsymbol{\mu}_0) \ln \left(\Pr_{x_{0:\tau}}(\mathcal{M}_0 = m | \mathcal{S}_0 \sim \boldsymbol{\mu}_0) \right) \\
&\quad - \sum_{m' \in \mathcal{M}} \Pr_{x_{0:\tau}}(\mathcal{M}_\tau = m' | \mathcal{S}_0 \sim \boldsymbol{\mu}_0) \ln \left(\Pr_{\mathbf{J}(x_{0:\tau})}(\mathcal{M}_0 = m^\dagger | \mathcal{S}_0 \sim \boldsymbol{\mu}_\tau^\dagger) \right) \\
&\quad + \sum_{m, m' \in \mathcal{M}} \Pr_{x_{0:\tau}}(\mathcal{M}_0 = m | \mathcal{S}_0 \sim \boldsymbol{\mu}_0) \Pr_{x_{0:\tau}}(\mathcal{M}_\tau = m' | \mathcal{S}_0 \sim \boldsymbol{\mu}_0, \mathcal{M}_0 = m) \\
&\quad \times \ln \left(\frac{\Pr_{x_{0:\tau}}(\mathcal{M}_\tau = m' | \mathcal{S}_0 \sim \boldsymbol{\mu}_0, \mathcal{M}_0 = m)}{\Pr_{\mathbf{J}(x_{0:\tau})}(\mathcal{M}_\tau = m^\dagger | \mathcal{S}_0 \sim \boldsymbol{\mu}_\tau^\dagger, \mathcal{M}_0 = m^\dagger)} \right) \\
&= \sum_{m \in \mathcal{M}} \boldsymbol{\mu}_0(m) \ln(\boldsymbol{\mu}_0(m)) - \sum_{m' \in \mathcal{M}} \boldsymbol{\mu}_\tau(m') \ln(\boldsymbol{\mu}_\tau^\dagger(m')) \\
&\quad + \sum_{m, m' \in \mathcal{M}} \boldsymbol{\mu}_0(m) \Pr_{x_{0:\tau}}(\mathcal{M}_\tau = m' | \mathcal{S}_0 \sim \boldsymbol{\mu}_0^{(m)}) \ln \left(\frac{\Pr_{x_{0:\tau}}(\mathcal{M}_\tau = m' | \mathcal{S}_0 \sim \boldsymbol{\mu}_0^{(m)})}{\Pr_{\mathbf{J}(x_{0:\tau})}(\mathcal{M}_\tau = m^\dagger | \mathcal{S}_0 \sim \boldsymbol{\mu}_\tau^{\dagger(m')})} \right) \\
&= -H(\mathcal{M}_0) + H(\mathcal{M}_\tau) + \sum_{m, m' \in \mathcal{M}} \boldsymbol{\mu}_0(m) d(m, m') \\
&= \Delta H(\mathcal{M}_t) + \sum_{m, m' \in \mathcal{M}} \boldsymbol{\mu}_0(m) d(m, m') . \tag{B3}
\end{aligned}$$

In the third-to-last equation above we used the fact that:

$$\boldsymbol{\mu}_\tau^\dagger(m^\dagger) = \boldsymbol{\mu}_\tau(m) ,$$

and we defined:

$$\begin{aligned}
d(m, m') &\equiv \Pr_{x_{0:\tau}}(\mathcal{M}_\tau = m' | \mathcal{S}_0 \sim \boldsymbol{\mu}_0^{(m)}) \\
&\quad \times \ln \left(\frac{\Pr_{x_{0:\tau}}(\mathcal{M}_\tau = m' | \mathcal{S}_0 \sim \boldsymbol{\mu}_0^{(m)})}{\Pr_{\mathbf{J}(x_{0:\tau})}(\mathcal{M}_\tau = m^\dagger | \mathcal{S}_0 \sim \boldsymbol{\mu}_\tau^{\dagger(m')})} \right) .
\end{aligned}$$

A more general derivation (*not* assuming that $m^\dagger \in \mathcal{M}$), fully leveraging Eq. (B1), yields Eq. (B3) with:

$$\begin{aligned}
d(m, m') &\equiv \Pr_{x_{0:\tau}}(\mathcal{M}_\tau = m' | \mathcal{S}_0 \sim \boldsymbol{\mu}_0^{(m)}) \\
&\quad \times \ln \left(\frac{\Pr_{x_{0:\tau}}(\mathcal{M}_\tau = m' | \mathcal{S}_0 \sim \boldsymbol{\mu}_0^{(m)})}{\Pr_{\mathbf{J}(x_{0:\tau})}(\mathcal{S}_\tau \in m^\dagger | \mathcal{S}_0 \sim \boldsymbol{\mu}_\tau^{\dagger(m')})} \right) .
\end{aligned}$$

This generalization would, for example, be useful in the analysis of tristable magnetic memory elements.

In the $m = m^\dagger$ case, where memories are stored via

time-symmetric variables, these expressions both simplify to:

$$d(m, m') = \Pr_{x_0:\tau}(\mathcal{M}_\tau = m' | \mathcal{S}_0 \sim \boldsymbol{\mu}_0^{(m)}) \\ \times \ln \left(\frac{\Pr_{x_0:\tau}(\mathcal{M}_\tau = m' | \mathcal{S}_0 \sim \boldsymbol{\mu}_0^{(m)})}{\Pr_{\mathbf{H}(x_0:\tau)}(\mathcal{M}_\tau = m | \mathcal{S}_0 \sim \boldsymbol{\mu}_\tau^{\dagger(m')})} \right).$$

This compares (i) the probability of transitioning from memory state m to m' to (ii) the probability of returning back to m upon reversal of time-odd variables (like momentum) and subsequent reversal of the control protocol. Above, $\boldsymbol{\mu}_t^{(m)} \equiv \delta_{\mathcal{S}_t \in m} \boldsymbol{\mu}_t / \sum_{s' \in m} \boldsymbol{\mu}_t(s')$ is the renormalized restriction of the microstate distribution $\boldsymbol{\mu}_t$ to the set of microstates represented by the memory m . Note that (despite the fact that $\boldsymbol{\mu}_\tau^\dagger(m^\dagger) = \boldsymbol{\mu}_\tau(m)$), generically $\boldsymbol{\mu}_\tau^{\dagger(m^\dagger)} \neq \boldsymbol{\mu}_\tau^{(m)}$. However, conveniently, metastable memory systems have: $\boldsymbol{\mu}_\tau^{\dagger(m)} \approx \boldsymbol{\pi}_{x_\tau}^{\dagger(m)} = \boldsymbol{\pi}_{x_\tau}^{(m)}$.

Appendix C: Transition-specific fluctuation theorem

Here, we verify the transition-specific version of Eq. (19). We start with the detailed fluctuation theorem for heat:

$$e^{\beta Q(s_0:\tau, x_0:\tau)} = \frac{\Pr_{x_0:\tau}(\mathcal{S}_{0:\tau} = s_0:\tau | \mathcal{S}_0 = s_0)}{\Pr_{\mathbf{H}(x_0:\tau)}(\mathcal{S}_{0:\tau} = \mathbf{H}(s_0:\tau) | \mathcal{S}_0 = s_\tau^\dagger)}.$$

We then utilize the First Law of thermodynamics (i.e., energy conservation):

$$E_{x_\tau}(s_\tau) - E_{x_0}(s_0) = W - Q,$$

together with a useful identity:

$$E_x(s) = -k_B T \ln(\boldsymbol{\pi}_x^{(m)}(s)) + F_x^{(m)},$$

if $s \in m$. This allows us to write:

$$W - \Delta F_x^{(m)} = Q + k_B T \Delta \ln(\boldsymbol{\pi}_x^{(m)}(s)).$$

Then we calculate:

$$\begin{aligned} & \langle e^{-\beta(W - \Delta F_x^{(m)})} \rangle_{\Pr_{x_0:\tau}(\mathcal{S}_{0:\tau} | \mathcal{M}_\tau = m', \mathcal{S}_0 \sim \boldsymbol{\pi}_{x_0}^{(m)})} \\ &= \langle e^{-\beta(Q - k_B T \Delta \ln(\boldsymbol{\pi}_x^{(m)}(s)))} \rangle_{\Pr_{x_0:\tau}(\mathcal{S}_{0:\tau} | \mathcal{M}_\tau = m', \mathcal{S}_0 \sim \boldsymbol{\pi}_{x_0}^{(m)})} \\ &= \sum_{s_0:\tau \in \mathcal{S}^{[0:\tau]}} \Pr_{x_0:\tau}(\mathcal{S}_{0:\tau} = s_0:\tau | \mathcal{M}_\tau = m', \mathcal{S}_0 \sim \boldsymbol{\pi}_{x_0}^{(m)}) \frac{\boldsymbol{\pi}_{x_\tau}^{(m')}(s_\tau)}{\boldsymbol{\pi}_{x_0}^{(m)}(s_0)} \frac{\Pr_{\mathbf{H}(x_0:\tau)}(\mathcal{S}_{0:\tau} = \mathbf{H}(s_0:\tau) | \mathcal{S}_0 = s_\tau^\dagger)}{\Pr_{x_0:\tau}(\mathcal{S}_{0:\tau} = s_0:\tau | \mathcal{S}_0 = s_0)} \\ &= \sum_{s_0:\tau \in m \mathcal{S}^{(0:\tau)} m'} \Pr_{x_0:\tau}(\mathcal{S}_{0:\tau} = s_0:\tau | \mathcal{M}_\tau = m', \mathcal{S}_0 \sim \boldsymbol{\pi}_{x_0}^{(m)}) \frac{\boldsymbol{\pi}_{x_\tau}^{(m')}(s_\tau)}{\boldsymbol{\pi}_{x_0}^{(m)}(s_0)} \frac{\Pr_{\mathbf{H}(x_0:\tau)}(\mathcal{S}_{0:\tau} = \mathbf{H}(s_0:\tau) | \mathcal{S}_0 = s_\tau^\dagger)}{\Pr_{x_0:\tau}(\mathcal{S}_{0:\tau} = s_0:\tau | \mathcal{S}_0 = s_0)} \\ &= \frac{1}{\Pr_{x_0:\tau}(\mathcal{M}_\tau = m' | \mathcal{S}_0 \sim \boldsymbol{\pi}_{x_0}^{(m)})} \sum_{s_0:\tau \in m \mathcal{S}^{(0:\tau)} m'} \Pr_{x_0:\tau}(\mathcal{S}_{0:\tau} = s_0:\tau | \mathcal{S}_0 \sim \boldsymbol{\pi}_{x_0}^{(m)}) \frac{\boldsymbol{\pi}_{x_\tau}^{(m')}(s_\tau)}{\boldsymbol{\pi}_{x_0}^{(m)}(s_0)} \frac{\Pr_{\mathbf{H}(x_0:\tau)}(\mathcal{S}_{0:\tau} = \mathbf{H}(s_0:\tau) | \mathcal{S}_0 = s_\tau^\dagger)}{\Pr_{x_0:\tau}(\mathcal{S}_{0:\tau} = s_0:\tau | \mathcal{S}_0 = s_0)} \\ &= \frac{1}{\Pr_{x_0:\tau}(\mathcal{M}_\tau = m' | \mathcal{S}_0 \sim \boldsymbol{\pi}_{x_0}^{(m)})} \sum_{s_0:\tau \in m \mathcal{S}^{(0:\tau)} m'} \boldsymbol{\pi}_{x_\tau}^{(m')}(s_\tau) \frac{\Pr_{\mathbf{H}(x_0:\tau)}(\mathcal{S}_{0:\tau} = \mathbf{H}(s_0:\tau) | \mathcal{S}_0 = s_\tau^\dagger)}{\Pr_{x_0:\tau}(\mathcal{S}_{0:\tau} = s_0:\tau | \mathcal{S}_0 = s_0)} \\ &= \frac{1}{\Pr_{x_0:\tau}(\mathcal{M}_\tau = m' | \mathcal{S}_0 \sim \boldsymbol{\pi}_{x_0}^{(m)})} \sum_{\mathbf{H}(s_0:\tau) \in m'^\dagger \mathcal{S}^{(0:\tau)} m^\dagger} \boldsymbol{\pi}_{x_\tau}^{(m')}(s_\tau^\dagger) \frac{\Pr_{\mathbf{H}(x_0:\tau)}(\mathcal{S}_{0:\tau} = \mathbf{H}(s_0:\tau) | \mathcal{S}_0 = s_\tau^\dagger)}{\Pr_{x_0:\tau}(\mathcal{S}_{0:\tau} = s_0:\tau | \mathcal{S}_0 = s_0)} \\ &= \frac{1}{\Pr_{x_0:\tau}(\mathcal{M}_\tau = m' | \mathcal{S}_0 \sim \boldsymbol{\pi}_{x_0}^{(m)})} \sum_{\mathbf{H}(s_0:\tau) \in m'^\dagger \mathcal{S}^{(0:\tau)} m^\dagger} \Pr_{\mathbf{H}(x_0:\tau)}(\mathcal{S}_{0:\tau} = \mathbf{H}(s_0:\tau) | \mathcal{S}_0 \sim \boldsymbol{\pi}_{x_\tau}^{(m')}) \\ &= \frac{1}{\Pr_{x_0:\tau}(\mathcal{M}_\tau = m' | \mathcal{S}_0 \sim \boldsymbol{\pi}_{x_0}^{(m)})} \sum_{s \in m^\dagger} \Pr_{\mathbf{H}(x_0:\tau)}(\mathcal{S}_\tau = s | \mathcal{S}_0 \sim \boldsymbol{\pi}_{x_\tau}^{(m')}) \\ &= \frac{\Pr_{\mathbf{H}(x_0:\tau)}(\mathcal{M}_\tau = m^\dagger | \mathcal{S}_0 \sim \boldsymbol{\pi}_{x_\tau}^{(m')})}{\Pr_{x_0:\tau}(\mathcal{M}_\tau = m' | \mathcal{S}_0 \sim \boldsymbol{\pi}_{x_0}^{(m)})}, \end{aligned}$$

where we used the fact that $\boldsymbol{\pi}_{x_\tau}^{(m')}(s_\tau) = \boldsymbol{\pi}_{x_\tau^\dagger}^{(m')}(s_\tau^\dagger)$.

Altogether, this leads to a useful transition-specific fluctuation theorem:

$$\langle e^{-\beta W} \rangle_{\text{Pr}_{x_0:\tau}(\mathcal{S}_{0:\tau}|\mathcal{M}_\tau=m', \mathcal{S}_0 \sim \pi_{x_0}^{(m)})} = e^{-\beta \Delta F_x^{(\mathcal{M})}} \frac{\text{Pr}_{\mathbf{R}(x_0:\tau)}(\mathcal{M}_\tau = m^\dagger | \mathcal{S}_0 \sim \pi_{x_\tau}^{(m^\dagger)})}{\text{Pr}_{x_0:\tau}(\mathcal{M}_\tau = m' | \mathcal{S}_0 \sim \pi_{x_0}^{(m)})}.$$

By Jensen's inequality, this yields:

$$\langle W \rangle_{\text{Pr}_{x_0:\tau}(\mathcal{S}_{0:\tau}|\mathcal{M}_\tau=m', \mathcal{S}_0 \sim \pi_{x_0}^{(m)})} \geq \Delta F_x^{(\mathcal{M})} + k_B T \ln \frac{\text{Pr}_{x_0:\tau}(\mathcal{M}_\tau = m' | \mathcal{S}_0 \sim \pi_{x_0}^{(m)})}{\text{Pr}_{\mathbf{R}(x_0:\tau)}(\mathcal{M}_\tau = m^\dagger | \mathcal{S}_0 \sim \pi_{x_\tau}^{(m^\dagger)})}.$$

Assuming time-symmetric control, this then implies that the minimal average work required of a memory transition is:

$$W_{\min}^{t\text{-sym}}(m \rightarrow m') = F_{x_0}^{(m')} - F_{x_0}^{(m)} + k_B T \Psi(m \rightarrow m').$$

These results exhibit similarity with those of Ref. [35], although the appearance of the local-equilibrium free energies is a new feature here. This has important implications for the work required of metastable memory transitions.

Appendix D: Four cases

To evaluate Eq. (15) there are four cases to consider. Assuming time-symmetric memories (such that $m^\dagger = m$), the four cases depend on whether $\mathcal{C}(m) = m'$ or $\neq m'$, and on whether $\mathcal{C}(m') = m$ or $\neq m$. Whatever implementation is used for the computation, it will result in some *actual* probability of error for each of the intended transitions: $\text{Pr}_{x_0:\tau}(\mathcal{M}_\tau = \mathcal{C}(m) | \mathcal{M}_0 = m) = 1 - \epsilon_m$. The reliability design constraint is that $\epsilon_m \leq \epsilon$ for all possible initial memories m , and that $\epsilon \ll 1$, so that errors are very improbable.

Given some implementation $x_{0:\tau}$, the actual probability of making a particular *accidental* memory transition is $\epsilon_{m \rightarrow m'}$ for $m' \neq \mathcal{C}(m)$. Since $\sum_{m' \in \mathcal{M} \setminus \{\mathcal{C}(m)\}} \epsilon_{m \rightarrow m'} = \epsilon_m \leq \epsilon$, we must have that $0 < \epsilon_{m \rightarrow m'} < \epsilon_m \leq \epsilon$. Let us use this to evaluate the four possible cases for $d(m, m')$:

1. $\mathcal{C}(m) = m'; \mathcal{C}(m') = m$:

$$\begin{aligned} d^{(1)}(m, m') &= (1 - \epsilon_m) \ln \left(\frac{1 - \epsilon_m}{1 - \epsilon_{m'}} \right) \\ &\geq (1 - \epsilon_m) \ln (1 - \epsilon_m) \\ &\geq (1 - \epsilon) \ln (1 - \epsilon) \\ &= (1 - \epsilon) \left(-\epsilon - \frac{1}{2}\epsilon^2 - \frac{1}{3}\epsilon^3 - \dots \right) \\ &= -\epsilon + \frac{1}{2}\epsilon^2 + \frac{1}{6}\epsilon^3 + \dots \\ &\geq -\epsilon + \frac{1}{2}\epsilon^2 \\ &\geq -\epsilon \\ &\approx 0 \end{aligned}$$

Similarly,

$$\begin{aligned} d^{(1)}(m, m') &= (1 - \epsilon_m) \ln \left(\frac{1 - \epsilon_m}{1 - \epsilon_{m'}} \right) \\ &\leq -\ln(1 - \epsilon_{m'}) \\ &\leq -\ln(1 - \epsilon) \\ &= \epsilon + \frac{1}{2}\epsilon^2 + \frac{1}{3}\epsilon^3 + \dots \\ &\approx 0 \end{aligned}$$

So $-\epsilon \leq d^{(1)}(m, m') \leq \epsilon + \frac{1}{2}\epsilon^2 + \mathcal{O}(\epsilon^3)$.

2. $\mathcal{C}(m) = m'; \mathcal{C}(m') \neq m$:

$$\begin{aligned} d^{(2)}(m, m') &= (1 - \epsilon_m) \ln \left(\frac{1 - \epsilon_m}{\epsilon_{m' \rightarrow m}} \right) \\ &\geq (1 - \epsilon) \ln \left(\frac{1 - \epsilon}{\epsilon_{m' \rightarrow m}} \right) \\ &\geq (1 - \epsilon) \ln \left(\frac{1 - \epsilon}{\epsilon} \right) \\ &\approx \ln(1/\epsilon) \end{aligned}$$

We also have:

$$\begin{aligned} d^{(2)}(m, m') &= (1 - \epsilon_m) \ln \left(\frac{1 - \epsilon_m}{\epsilon_{m' \rightarrow m}} \right) \\ &\leq \ln(1/\epsilon_{m' \rightarrow m}) \end{aligned}$$

So, $\ln(\epsilon^{-1}) \lesssim d^{(2)}(m, m') \leq \ln(\epsilon_{m' \rightarrow m}^{-1})$.

3. $\mathcal{C}(m) \neq m'; \mathcal{C}(m') = m$:

$$\begin{aligned} d^{(3)}(m, m') &= \epsilon_{m \rightarrow m'} \ln \left(\frac{\epsilon_{m \rightarrow m'}}{1 - \epsilon_{m'}} \right) \\ &> \epsilon_{m \rightarrow m'} \ln \epsilon_{m \rightarrow m'} \\ &\approx 0 \end{aligned}$$

Also:

$$d^{(3)}(m, m') = \epsilon_{m, m'} \ln \left(\frac{\epsilon_{m, m'}}{1 - \epsilon_{m'}} \right) < 0 .$$

So, $\epsilon_{m \rightarrow m'} \ln \epsilon_{m \rightarrow m'} < d^{(3)}(m, m') < 0$.

4. $\mathcal{C}(m) \neq m'$; $\mathcal{C}(m') \neq m$:

$$\begin{aligned} d^{(4)}(m, m') &= \epsilon_{m \rightarrow m'} \ln \left(\frac{\epsilon_{m \rightarrow m'}}{\epsilon_{m' \rightarrow m}} \right) \\ &< \epsilon_{m \rightarrow m'} \ln \left(\frac{1}{\epsilon_{m' \rightarrow m}} \right) \\ &\approx 0 , \end{aligned}$$

assuming that the errors $\epsilon_{m \rightarrow m'}$ and $\epsilon_{m' \rightarrow m}$ are on the same order of magnitude. Also:

$$\begin{aligned} d^{(4)}(m, m') &= \epsilon_{m \rightarrow m'} \ln \left(\frac{\epsilon_{m \rightarrow m'}}{\epsilon_{m' \rightarrow m}} \right) \\ &> \epsilon_{m \rightarrow m'} \ln \epsilon_{m \rightarrow m'} \\ &\approx 0 . \end{aligned}$$

So, $\epsilon_{m \rightarrow m'} \ln \epsilon_{m \rightarrow m'} < d^{(4)}(m, m') < -\epsilon_{m \rightarrow m'} \ln \epsilon_{m' \rightarrow m}$.

Case 2 is the only one resulting in divergent dissipation with increasing reliability.

However, due to the ratio of error rates in Case 4, its behavior in the low-error limit deserves further analysis.

On the one hand, suppose $\epsilon_{m' \rightarrow m} > \epsilon_{m \rightarrow m'}$. Let $r \equiv \epsilon_{m \rightarrow m'} / \epsilon_{m' \rightarrow m} < 1$. Then:

$$d^{(4)}(m, m') = \epsilon_{m \rightarrow m'} \ln \frac{\epsilon_{m \rightarrow m'}}{\epsilon_{m' \rightarrow m}} = \epsilon_{m' \rightarrow m} r \ln r .$$

If we define the function $f(r) = r \ln r$, then:

$$\begin{aligned} f'(r) &= \ln r + 1 , \\ f'(r^*) &= 0 \implies r^* = e^{-1} , \end{aligned}$$

and:

$$f(r^*) = -e^{-1} .$$

$f(0) = f(1) = 0$ so f 's local minimum is at e^{-1} . So:

$$d^{(4)}(m, m') = \epsilon_{m' \rightarrow m} r \ln r \geq -\epsilon_{m' \rightarrow m} e^{-1} .$$

However, $\epsilon \geq \epsilon_{m' \rightarrow m}$, so:

$$d^{(4)}(m, m') \geq -\epsilon e^{-1} .$$

And, since $f(r) \leq 0$ for $0 \leq r \leq 1$,

$$0 \geq d^{(4)}(m, m') \geq -\epsilon e^{-1} .$$

If, on the other hand, $\epsilon_{m \rightarrow m'} > \epsilon_{m' \rightarrow m}$, then Case 4 will imply some extra dissipation, although it will still be on the order of ϵ so long as $\epsilon_{m \rightarrow m'}$ and $\epsilon_{m' \rightarrow m}$ are within several orders of magnitude.

Appendix E: Langevin dynamics for erasure

The following documents the dynamics and methods of our analysis for the simulations described in Sec. IV A 2.

We consider a one-dimensional particle with position and momentum in an external potential and in thermal contact with the environment at temperature T . As a function of position q and time t , the potential takes the form:

$$V(q, t) = aq^4 - b_0 b_f(t) q^2 + c_0 c_f(t) q ,$$

with constants $a, b_0, c_0 > 0$. The functions $b_f(t)$ and $c_f(t)$ evolve in a piecewise linear, cyclic, and time-symmetric manner according to Table I, where $t_0, t_1, \dots, t_7 = 0, \frac{\tau}{12}, \frac{3\tau}{12}, \frac{5\tau}{12}, \frac{7\tau}{12}, \frac{9\tau}{12}, \frac{11\tau}{12}, \tau$. The potential thus begins and ends in a symmetric double-well configuration with each well defining a memory state. During the protocol, though, the number of metastable regions is temporarily reduced to one.

t	t_0	t_1	t_2	t_3	t_4	t_5	t_6	t_7
$b_f(t)$	1	1	$\frac{t_3 - t_2}{t_3 - t_2}$	0	$\frac{t - t_4}{t_5 - t_4}$	1	1	
$c_f(t)$	0	$\frac{t - t_1}{t_2 - t_1}$	1	1	1	$\frac{t_6 - t}{t_6 - t_5}$	0	

TABLE I. Erasure protocol.

We simulate the motion of the particle with underdamped Langevin dynamics:

$$\begin{aligned} dq &= v dt \\ m dv &= - \left(\frac{\partial}{\partial q} V(q, t) + \lambda v \right) dt + \sqrt{2k_B T \lambda} r(t) \sqrt{dt} , \end{aligned}$$

where k_B is Boltzmann's constant, λ is the coupling between the thermal environment and particle, m is the particle's mass, and $r(t)$ is a memoryless Gaussian random variable with $\langle r(t) \rangle = 0$ and $\langle r(t) r(t') \rangle = \delta(t - t')$.

The work done on a single particle over the course of the

protocol with trajectory $\{q(t)\}_t$ is then:

$$W = \int_0^\tau dt \frac{\partial V(q, t)}{\partial t} \Big|_{q=q(t)} .$$

To help simulate a wide variety of protocols, we first nondimensionalize the equations of motion. We define the following nondimensional variables:

$$q' = \sqrt{\frac{2a}{b_0}} q , \quad t' = \frac{2ak_B T}{b_0 \lambda} t , \quad v' = \frac{\lambda}{k_B T} \sqrt{\frac{b_0}{2a}} v , \quad \text{and} \\ V' = \frac{1}{k_B T} V .$$

Note that the position scale $\sqrt{b_0/2a}$ is the position distance from zero to either well minima in the default potential $V(\cdot, 0) = V(\cdot, \tau)$. Substitution then provides the following nondimensional equations:

$$dq' = v' dt' \\ m' dv' = - \left(\frac{\partial}{\partial q'} V'(q', t') + v' \right) dt' + \sqrt{2} r(t') \sqrt{dt'} ,$$

with:

$$m' = \frac{2amk_B T}{b_0 \lambda^2} ,$$

which is our first nondimensional parameter to specify. The nondimensional potential can be expressed as:

$$V'(q', t') = \alpha \left(q'^4 - 2b'_f(t') q'^2 + \zeta c'_f(t') q' \right) ,$$

where:

$$\alpha = \frac{b_0^2}{4ak_B T} \quad \text{and} \quad \zeta = c_0 \sqrt{\frac{2a}{b_0^3}}$$

are two more nondimensional parameters and:

$$b'_f(t') = b_f \left(\frac{2ak_B T}{b_0 \lambda} t \right) \quad \text{and} \quad c'_f(t') = c_f \left(\frac{2ak_B T}{b_0 \lambda} t \right)$$

simply express b_f and c_f with the nondimensional time as input. The fourth and final nondimensional parameter is the nondimensional total time:

$$\tau' = \frac{2ak_B T}{b_0 \lambda} \tau .$$

To construct Fig. 10, we simulate 735 different protocols, determined by all combinations of the following values for the four nondimensional parameters: $m' \in \{0.25, 1.0, 4.0\}$, $\alpha \in \{2, 4, 7, 10, 12\}$, $\zeta \in \{0.1, 0.2, 0.3, 0.4, 0.5, 0.6, 0.7\}$, and $\tau' \in \{4, 8, 16, 32, 64, 128, 256\}$. 100,000 trials of each parameter set were simulated. To update the position

and velocity of the particle at each time step, we used the fourth-order Runge-Kutta method for the deterministic portion and the simple Euler method in combination with a Gaussian number generator for the stochastic portion.

To determine this time step size, we considered a range of possible time steps for 81 of the possible 735 parameter sets and looked for convergence of the sampled average works and maximum errors ϵ , again using 100,000 trials per parameter set. The maximum errors were stable over the whole range of tested step sizes. Looking with decreasing step size, the final step size was chosen when the average works stopped fluctuating within 5 sigma of their statistical errors for all 81 parameter sets.

The error bars presented for the average works in Fig. 10 were then generously set to be 5 times the estimated statistical errors, which were each obtained by dividing the sampled standard deviation by the square root of the number of trials. Error bars for the maximum errors were set to be the statistical errors of ϵ_L or ϵ_R , depending on which was the maximum, whose statistical errors were obtained by assuming binomial statistics.

Appendix F: Minimal dissipation in the time-symmetric universal NAND gate

Let us consider the implications for the common logic gates that serve as the building blocks for practical computers. Recall that the simple NAND gate is sufficient for universal computation. It is therefore worthwhile to consider what dissipation is commonly incurred in such important logic gates—and consider how this dissipation can be avoided.

To address this, consider a physical implementation of the memory components of a NAND gate, where we explicitly consider two memory elements whose memory states are to be used as the input for the NAND gate and another memory element that will store the value of the output. We assume that only the output is over-written during the computation—the input memory states may be kept around for later use.

Note that this is already a particular physical model of the NAND computation—indeed, alternatives exist such as storing the output in the location of one of the former inputs by over-writing one of the inputs. However, we analyze the proposed two-input-one-output model here since it is arguably the most relevant to the typical desired use of a NAND gate. Other ancillary memory elements may be used in the computation as in Ref. [58] but, since they will be returned to their original state by the computation's end, these ancillary memories do not need to result in any explicit additional dissipation

dependence—although they can influence the dissipation through their implicit effect on the net errors in operating on the memory-elements of interest—and can be left implicit in the self-consistency of the current analysis.

Each of the three explicitly-considered memory elements is assumed to be bistable; i.e., each has two metastable regions of state space.¹¹ Let the microstate of each memory element be specified by its position in the interval $(-\pi, \pi]$. Between computations, including at $t = 0$ and $t = \tau$, the metastable regions for each memory element are $\mathbf{0} \equiv (-\pi, 0]$ and $\mathbf{1} \equiv (0, \pi]$ which gives a natural partition for the memory states.

The microstate of the memory system at any time t can be treated as a composite random variable $\mathcal{S}_t = (\mathcal{S}_t^{(\text{in}1)}, \mathcal{S}_t^{(\text{in}2)}, \mathcal{S}_t^{(\text{out})})$ with $\mathcal{S}_t^{(\cdot)} \in (-\pi, \pi]$. Similarly, the memory state is the composite random variable $\mathcal{M}_t = (\mathcal{M}_t^{(\text{in}1)}, \mathcal{M}_t^{(\text{in}2)}, \mathcal{M}_t^{(\text{out})})$ with $\mathcal{M}_t^{(\cdot)} \in \{\mathbf{0}, \mathbf{1}\}$ corresponding to the two metastable regions for each memory element. Thus, the joint state-space $\mathcal{S} = \mathbb{R}_{(-\pi, \pi]}^3$ has eight metastable regions, which we identify as the joint memory system's eight memory states: $\mathcal{M} = \{m_{\mathbf{000}}, m_{\mathbf{001}}, m_{\mathbf{010}}, \dots, m_{\mathbf{111}}\}$ where each memory state is labeled according to its corresponding region of state-space: $m_{jkl} = \{s \in \mathcal{S} : s^{(\text{in}1)} \in (-\pi + j\pi, j\pi], s^{(\text{in}2)} \in (-\pi + k\pi, k\pi], s^{(\text{out})} \in (-\pi + \ell\pi, \ell\pi]\}$. That is, each of the memory states is one of the octants of state space.

¹¹ For example, each memory element may be realized physically by the bistable magnetic moment of a superparamagnetic nanocrystal in the so-called ‘blocked’ regime where the Néel relaxation time between metastable regions is much larger than the timescale of computation in the system. We can assume that there is sufficient uniaxial anisotropy (or sufficiently low temperature) to create a potential barrier many times the thermal energy between the potential wells of the two metastable regions. Alternatively, the memory elements can be realized experimentally as bistable wells created by optical tweezers. This latter option is less scalable but sufficient for initial experiments.

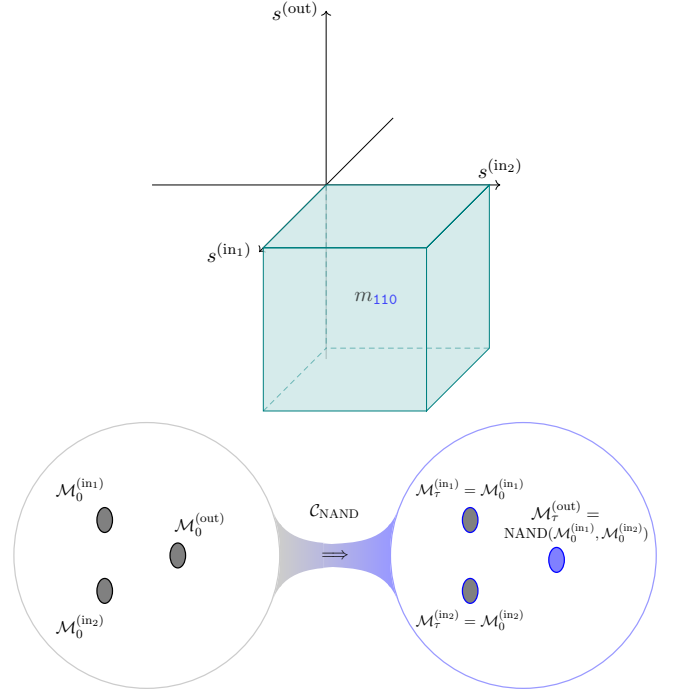


FIG. 11. Composite state space, memory states, and computation associated with the logical NAND operation. [Reproduced with permission (with minor modification) from Ref. [5].]

The NAND computation $\mathcal{C}_{\text{NAND}}$ is given by the mappings:

$$\begin{array}{ll} \mathbf{000} \mapsto \mathbf{001} & \mathbf{001} \mapsto \mathbf{001} \\ \mathbf{010} \mapsto \mathbf{011} & \mathbf{011} \mapsto \mathbf{011} \\ \mathbf{100} \mapsto \mathbf{101} & \mathbf{101} \mapsto \mathbf{101} \\ \mathbf{110} \mapsto \mathbf{110} & \mathbf{111} \mapsto \mathbf{110} \end{array}$$

For arbitrary initial correlation among the memory elements before the computation, the change in memory entropy is:

$$\begin{aligned} \Delta H(\mathcal{M}_t) &= H(\mathcal{M}_\tau^{(\text{in}1)}, \mathcal{M}_\tau^{(\text{in}2)}, \mathcal{M}_\tau^{(\text{out})}) - H(\mathcal{M}_0^{(\text{in}1)}, \mathcal{M}_0^{(\text{in}2)}, \mathcal{M}_0^{(\text{out})}) \\ &\approx H(\mathcal{M}_0^{(\text{in}1)}, \mathcal{M}_0^{(\text{in}2)}, \mathcal{M}_\tau^{(\text{out})}) - H(\mathcal{M}_0^{(\text{in}1)}, \mathcal{M}_0^{(\text{in}2)}, \mathcal{M}_0^{(\text{out})}) \\ &\approx H(\mathcal{M}_0^{(\text{in}1)}, \mathcal{M}_0^{(\text{in}2)}) - H(\mathcal{M}_0^{(\text{in}1)}, \mathcal{M}_0^{(\text{in}2)}, \mathcal{M}_0^{(\text{out})}) \\ &= -H(\mathcal{M}_0^{(\text{out})} | \mathcal{M}_0^{(\text{in}1)}, \mathcal{M}_0^{(\text{in}2)}) , \end{aligned}$$

where we made the approximation that ϵ is very small. The entropy $H(\mathcal{M}_0^{(\text{out})} | \mathcal{M}_0^{(\text{in}1)}, \mathcal{M}_0^{(\text{in}2)})$ is the Landauer bound for the NAND gate—a result of interest in its own right. Here, we use it to provide the $\Delta H(\mathcal{M}_t)$ needed for our calculation of dissipation for time-symmetric implementations of NAND.

It should be noted that, by the definition of $\mathcal{C}_{\text{NAND}}$, half

of the memory states map to themselves. The other half never get mapped back to themselves upon iteration of the computation. The reciprocity coefficient is therefore:

$$\begin{aligned} & \langle [\mathcal{C}_{\text{NAND}}(\mathcal{C}_{\text{NAND}}(\mathcal{M}_0)) \neq \mathcal{M}_0] \rangle_{\mathcal{M}_0} \\ &= \mu_0(000) + \mu_0(010) + \mu_0(100) + \mu_0(111) . \end{aligned}$$

Together with Eq. (30), these give the general lower bound for NAND gate dissipation when a time-symmetric protocol is used and the memory elements are initially correlated.

In the simpler case where the memory elements are initiated with individual biases towards **0** or **1**, but are otherwise uncorrelated with each other, the NAND dissipation somewhat simplifies, since then:

$$\begin{aligned} \Delta H(\mathcal{M}_t) &\approx -H(\mathcal{M}_0^{(\text{out})} | \mathcal{M}_0^{(\text{in}_1)}, \mathcal{M}_0^{(\text{in}_2)}) \\ &= -H(\mathcal{M}_0^{(\text{out})}) \\ &= -H_b(b_0^{(\text{out})}) , \end{aligned}$$

where $b_0^{(\text{out})}$ is the initial bias of the output bit to be

overwritten.

In this latter uncorrelated case, the time-symmetric NAND dissipation resembles the dissipation that would be expected simply from bit erasure of the output bit. The primary difference is that the probability of overwriting the output bit now depends intricately on a function $\langle [\mathcal{C}_{\text{NAND}}(\mathcal{C}_{\text{NAND}}(\mathcal{M}_0)) \neq \mathcal{M}_0] \rangle_{\mathcal{M}_0}$ of the distribution over the joint memory state of all memory elements which is not separable even when the joint distribution over memory elements is separable.

It should be noted that, even in the case of biased but uncorrelated initialization of the memory, the initialization statistics would need to be taken into account to make the time-symmetric physical implementation as thermodynamically efficient as possible. Interestingly, even in the case of time-asymmetric protocols, it has been found that the initialization statistics must be taken into account for thermodynamic efficiency of the NAND gate [5]. Thus, the impetus to match the input statistics is somewhat of a separate generic issue in addition to the lesson of extra dissipation that generically accompanies time-symmetric implementation of reliable computation.

-
- [1] C. H. Bennett. Thermodynamics of computation—A review. *Intl. J. Theo. Phys.*, 21:905, 1982. [2](#), [10](#), [13](#), [18](#)
 - [2] O. J. E. Maroney. Generalizing Landauer’s principle. *Phys. Rev. E*, 79:031105, Mar 2009. [2](#), [11](#), [13](#)
 - [3] T. Sagawa. Thermodynamic and logical reversibilities revisited. *J. Stat. Mech. Th. Exp.*, 2014(3):P03025, 2014. [13](#)
 - [4] J. M. R. Parrondo, J. M. Horowitz, and T. Sagawa. Thermodynamics of information. *Nature Physics*, 11(2):131, 2015. [11](#)
 - [5] P. M. Riechers. Transforming metastable memories: The nonequilibrium thermodynamics of computation. In D. Wolpert, C. Kempes, P. Stadler, and J. Grochow, editors, *The Energetics of Computing in Life and Machines*. SFI Press, 2019. [2](#), [9](#), [13](#), [21](#), [31](#), [32](#)
 - [6] P. Salamon and R. S. Berry. Thermodynamic length and dissipated availability. *Phys. Rev. Lett.*, 51:1127–1130, Sep 1983. [2](#)
 - [7] D. A. Sivak and G. E. Crooks. Thermodynamic metrics and optimal paths. *Phys. Rev. Lett.*, 108:190602, May 2012.
 - [8] P. R. Zulkowski and M. R. DeWeese. Optimal finite-time erasure of a classical bit. *Phys. Rev. E*, 89(5):052140, 2014.
 - [9] M. VS. Bonança and S. Deffner. Optimal driving of isothermal processes close to equilibrium. *J. Chem. Phys.*, 140(24):244119, 2014.
 - [10] D. Mandal and C. Jarzynski. Analysis of slow transitions between nonequilibrium steady states. *J. Stat. Mech. Th. Exp.*, 2016(6):063204, 2016.
 - [11] A. B. Boyd, A. Patra, C. Jarzynski, and J. P. Crutchfield. Shortcuts to thermodynamic computing: The cost of fast and faithful information processing. arXiv:1812.11241. [2](#), [21](#)
 - [12] A. P. Chandrakasan, S. Sheng, and R. W. Brodersen. Low-power CMOS digital design. *IEEE J. Solid-State Circ.*, 27(4):473–484, April 1992. [2](#)
 - [13] A. Iyer and D. Marculescu. Power efficiency of voltage scaling in multiple clock, multiple voltage cores. In *Proc. 2002 IEEE/ACM Intl. Cong. Computer-aided Design*, pages 379–386. ACM, 2002. [2](#)
 - [14] R. D. Astumian. How molecular motors work—insights from the molecular machinist’s toolbox: The Nobel Prize in Chemistry 2016. *Chemical Sci.*, 8(2):840–845, 2017. [2](#), [19](#)
 - [15] A. I. Brown and D. A. Sivak. Toward the design principles of molecular machines. arXiv:1701.04868. [2](#)
 - [16] L. Zhang, V. Marcos, and D. A. Leigh. Molecular machines with bio-inspired mechanisms. *Proc. Natl. Acad. Sci.*, 115(38):9397–9404, 2018. [2](#)
 - [17] E. H. Feng and G. E. Crooks. Length of time’s arrow. *Phys. Rev. Lett.*, 101:090602, Aug 2008. [2](#), [19](#)
 - [18] R. Landauer. Irreversibility and heat generation in the computing process. *IBM J. Res. Develop.*, 5(3):183–191, 1961. [2](#), [13](#), [15](#)
 - [19] G. E. Crooks. Nonequilibrium measurements of free energy differences for microscopically reversible markovian systems. *J. Stat. eistical hysics*, 90(5-6):1481–1487, 1998. [3](#), [4](#)
 - [20] G. E. Crooks. Entropy production fluctuation theorem

- and the nonequilibrium work relation for free energy differences. *Phys. Rev. E*, 60:2721–2726, 1999. 3
- [21] C. Jarzynski. Hamiltonian derivation of a detailed fluctuation theorem. *J. Stat. Physics*, 98(1-2):77–102, 2000. 3, 4
- [22] U. Seifert. Entropy production along a stochastic trajectory and an integral fluctuation theorem. *Phys. Rev. Lett.*, 95:040602, Jul 2005. 3
- [23] M. Esposito and C. Van den Broeck. Second law and Landauer principle far from equilibrium. *Eur. Phys. Lett.*, 95(4), 2011. 3
- [24] T. M. Cover and J. A. Thomas. *Elements of Information Theory*. Wiley-Interscience, New York, second edition, 2006. 4, 5, 22, 25
- [25] M. Esposito. Stochastic thermodynamics under coarse graining. *Phys. Rev. E*, 85(4):041125, 2012. 4, 7
- [26] J. M. R. Parrondo, J. M. Horowitz, and T. Sagawa. Thermodynamics of information. *Nature Physics*, 11(2):131–139, February 2015. 4, 9, 13
- [27] R. Kawai, J. M. R. Parrondo, and C. Van den Broeck. Dissipation: The phase-space perspective. *Phys. Rev. Lett.*, 98:080602, 2007. 4, 5, 24
- [28] E. Roldan and J. M. R. Parrondo. Estimating dissipation from single stationary trajectories. *Phys. Rev. Lett.*, 105(150607), 2010.
- [29] J. Horowitz and C. Jarzynski. Illustrative example of the relationship between dissipation and relative entropy. *Phys. Rev. E*, 79(021106), 2009. 4
- [30] A. Gomez-Marín, J. M. R. Parrondo, and C. Van den Broeck. Lower bounds on dissipation upon coarse graining. *Phys. Rev. E*, 78(1):011107, 2008. 5, 24
- [31] E. Roldan and J. M. R. Parrondo. *Estimating dissipation from single stationary trajectories*. PhD thesis, Universidad Complutense de Madrid, 28040 Madrid, Spain, September 2010. 5, 24
- [32] Y. Jun, M. Gavrilov, and J. Bechhoefer. High-precision test of Landauer’s principle. *Phys. Rev. Lett.*, 113:190601, 2014. 6, 15
- [33] A. B. Boyd, D. Mandal, and J. P. Crutchfield. Thermodynamics of modularity: Structural costs beyond the Landauer bound. *Phys. Rev. X*, 8(031036), August 2018. 9, 21
- [34] A. Kolchinsky and D. H. Wolpert. Dependence of dissipation on the initial distribution over states. *J. Stat. Mech. Th. Exp.*, 2017(8):083202, 2017. 9
- [35] J. L. England. Statistical physics of self-replication. *J. Chem. Physics*, 139(12):121923, 2013. 9, 28
- [36] G. Wimsatt, O.-P. Saira, A. B. Boyd, M. H. Matheny, S. Han, M. L. Roukes, and J. P. Crutchfield. Harnessing fluctuations in thermodynamic computing via time-reversal symmetries. *arXiv:1906.11973*. 10
- [37] J. Hong, B. Lambson, S. Dhuey, and J. Bokor. Experimental test of Landauer’s principle in single-bit operations on nanomagnetic memory bits. *Sci. Adv.*, 2:e1501492, 2016. 15
- [38] S. Deffner and C. Jarzynski. Information processing and the second law of thermodynamics: An inclusive, Hamiltonian approach. *Phys. Rev. X*, 3:041003, 2013. 16, 21
- [39] R. Dillenschneider and E. Lutz. Memory erasure in small systems. *Phys. Rev. Lett.*, 102:210601, May 2009. 18
- [40] Y. Jun, M. Gavrilov, and J. Bechhoefer. High-precision test of Landauer’s principle in a feedback trap. *Phys. Rev. Lett.*, 113:190601, Nov 2014. 18
- [41] P. Shivakumar, M. Kistler, S. W. Keckler, D. Burger, and L. Alvisi. Modeling the effect of technology trends on the soft error rate of combinational logic. In *Dependable Systems and Networks, 2002. DSN 2002. Proceedings. International Conference on*, pages 389–398. IEEE, 2002. 18
- [42] E. Fredkin and T. Toffoli. Conservative logic. In *Collision-based computing*, pages 47–81. Springer, 2002. 18
- [43] P. M. Riechers and J. P. Crutchfield. Fluctuations when driving between nonequilibrium steady states. *J. Stat. Physics*, 168(4):873–918, 2017. 19
- [44] T. R. Gingrich, J. M. Horowitz, N. Perunov, and J. L. England. Dissipation bounds all steady-state current fluctuations. *Phys. Rev. Lett.*, 116:120601, Mar 2016. 19
- [45] J. J. Hopfield. Kinetic proofreading: A new mechanism for reducing errors in biosynthetic processes requiring high specificity. *Proc. Natl. Acad. Sci.*, 71(10):4135–4139, 1974. 20
- [46] Charles H. Bennett. Dissipation-error tradeoff in proofreading. *Biosystems*, 11(2):85 – 91, 1979.
- [47] A. Murugan, D. A. Huse, and S. Leibler. Speed, dissipation, and error in kinetic proofreading. *Proc. Natl. Acad. Sci.*, 109(30):12034–12039, 2012. 21
- [48] P. Sartori and S. Pigolotti. Thermodynamics of error correction. *Phys. Rev. X*, 5:041039, Dec 2015. 20
- [49] J. M. Horowitz, K. Zhou, and J. L. England. Minimum energetic cost to maintain a target nonequilibrium state. *Phys. Rev. E*, 95:042102, Apr 2017. 20
- [50] T. E. Ouldridge, C. C. Govern, and P. R. ten Wolde. Thermodynamics of computational copying in biochemical systems. *Phys. Rev. X*, 7(2):021004, 2017. 20
- [51] L. Brillouin. *Science and Information Theory*. Academic Press, New York, 1956. 20
- [52] K.-L. Stein. Noise-induced error rate as limiting factor for energy per operation in digital ICs. *IEEE J. Solid State Circuits*, SC-12(5):527–530, 1977. 20, 21
- [53] R. Muller, H.J. Pfeiderer, and K.U. Stein. Energy per logic operation in integrated circuits: Definition and determination. *IEEE J. Solid-State Circ.*, 11(5):657–661, 1976. 21
- [54] J. von Neumann. Probabilistic logics and the synthesis of reliable organisms from unreliable components. In C. E. Shannon and J. McCarthy, editors, *Automata Studies*, number 34 in Annals of Mathematical Studies, pages 329–378. Princeton University Press, Princeton, New Jersey, 1956. 21
- [55] G. Lan, P. Sartori, S. Neumann, V. Sourjik, and Y. Tu. The energy–speed–accuracy trade-off in sensory adaptation. *Nature Physics*, 8(5):422, 2012. 21
- [56] P. R. Zulkowski and M. R. DeWeese. Optimal finite-time erasure of a classical bit. *Phys. Rev. E*, 89:052140, 2014.
- [57] S. Lahiri, J. Sohl-Dickstein, and S. Ganguli. A universal tradeoff between power, precision and speed in physical

communication. *arXiv:1603.07758*. [21](#)

[58] J. A. Owen, A. Kolchinsky, and D. H. Wolpert. Number

of hidden states needed to physically implement a given conditional distribution. *New J. Physics*, 21:013022, 2018. [30](#)